

BIOMECHANICS OF TURNING MANOEUVRES IN STELLER SEA LIONS
(*EUMETOPIAS JUBATUS*)

by

OLIVIER CHENEVAL

B.Sc., Université du Québec à Montréal (UQÀM), 1998

A THESIS SUBMITTED IN PARTIAL FULFILLMENT OF
THE REQUIREMENTS FOR THE DEGREE OF

MASTER OF SCIENCE

in

THE FACULTY OF GRADUATE STUDIES

Zoology

THE UNIVERSITY OF BRITISH COLUMBIA

May 2005

ABSTRACT

Otariids such as the Steller sea lion (*Eumetopias jubatus*) are among the most manoeuvrable of marine mammals (expressed as a minimum turning radius and speed during manoeuvres). They evolved in terrestrial and aquatic environments that are structurally complex, and feed on prey that are an order of magnitude smaller than themselves. Compared to other aquatic organisms, Steller sea lions have an unstable body design and are presumed to invoke swimming techniques that reflect their need to be highly manoeuvrable. Detailed information was experimentally obtained about the turning techniques employed by otariids through jointly analysing kinematic and kinetic parameters measured from video recordings of three captive Steller sea lions. Centripetal force and thrust production were determined by examining body movements throughout a series of turns. Results showed that most of the thrust was produced during the power phase of the stroke cycle of the pectoral flippers. As opposed to previous findings, very little or no thrust was generated during initial abduction of the pectoral flippers and during the final drag-based paddling style of the stroke cycle. Peak of the thrust force was reached halfway through the power phase, while the centripetal force reached its maximum value at the beginning of the power phase. Kinematic aspects of the manoeuvres changed with the tightness of the turns and the initial velocities. The degree of dorsal flexion of the body changed with the turning radius and the degree of flipper abduction varied with swimming speed. However, the general manoeuvring technique and turning sequence remained the same in all the recorded manoeuvres. Contrasting the turning performance of the Steller sea lion with a simple dynamic model of unpowered manoeuvres in aquatic animals showed significant departures from model predictions due to the hydrodynamic effects of body movements. Overall, the turning sequence of the Steller sea lion was found to be very consistent, and their manoeuvrability was found to come from their ability to vary the duration and intensity of movements within the turning sequence.

TABLE OF CONTENTS

ABSTRACT.....	II
LIST OF TABLES	IV
LIST OF FIGURES.....	V
ACKNOWLEDGEMENTS.....	VI
INTRODUCTION.....	1
MATERIALS AND METHODS	4
Morphology	4
Experimental set-up	10
Video analysis.....	12
RESULTS	16
Morphology	16
Kinematics	19
Kinetics.....	26
DISCUSSION	32
Morphology	32
Kinematic analysis.....	37
Kinetic analysis.....	48
CONCLUSIONS.....	54
REFERENCES	56

LIST OF TABLES

Table 1: Mass of the three female Steller sea lions on the day of the filmed trials	17
Table 2: Morphological data of the three female Steller sea lions.....	18
Table 3: Sequence of movements performed by SL3 during a 180 degrees turn.....	23
Table 3 (continued): Sequence of movements performed by SL1 and SL2 during a 180 degrees turn	24
Table 4: Mean kinetic parameters for the SL3, SL2, and SL1	31

LIST OF FIGURES

Fig. 1:	3-D representation of the body of SL3 as obtained from girth measurements	5
Fig. 2:	Lifetime variation of 4 girth measurements as a function of body mass	7
Fig. 3:	On-screen morphological measurements of the left pectoral flipper of SL3	9
Fig. 4:	On-screen morphological measurements of the left pelvic flipper of SL3.....	9
Fig. 5:	Schematic of the experimental set-up.	11
Fig. 6:	Sequence of movements based on turn H128 performed by SL3.....	22
Fig. 7:	Relationship between turning radius and the degree of body curvature of three Steller sea lions performing a 180 degrees turn	25
Fig. 8:	Trajectory and speed profile of the shoulder, centre of gravity, and hip markers of a Steller sea lion performing a 180 degrees turn	29
Fig. 9:	Tangential and normal acceleration profiles of the shoulder, the centre of gravity, and hip markers of a Steller sea lion performing a 180 degrees turn	30
Fig. 10:	Trajectory of the nose and shoulder of a sea lion performing a 180 degrees turn	44
Fig. 11:	Comparison of the speed profiles of the shoulder, centre of gravity, and hip markers with the predictions of a theoretical model.....	45
Fig. 12:	Comparison of the speed profiles of the shoulder, centre of gravity, and hip markers of a Steller sea lion performing a fast and a slow 180 degrees turn.....	46
Fig. 13:	Relative turning radius and average turning speed of three Steller sea lions in comparison to California sea lions.....	47

ACKNOWLEDGEMENTS

I would like to acknowledge my thesis advisors, Dr. Andrew W. Trites and Dr. Robert W. Blake for their support during this project. Dr. Robert W. Blake was extremely helpful and supportive during the analysis and provided me with lab space. Dr. David A. S. Rosen was very accommodating of my research needs at the Vancouver Aquarium.

I would like to acknowledge the Vancouver Aquarium for providing research facilities and the staff for their help. I especially want to thank the Steller team at the Vancouver Aquarium: Rebecca Barrick and Chad Nordstrom, as well as the sea lion trainers: Shawn Carrier, Andrew Irvine, Billy Lasby, Vance Mercer, Troy Neale, Nigel Waller, and Gwyneth Shephard for their precious help and support. Thanks also to all the staff, colleagues and fellow students in the Marine Mammal Research Unit who provided help on frequent basis. This work was partially funded by NSERC, and grants to the North Pacific Universities Marine Mammal Research Consortium from NOAA and the North Pacific Marine Science Foundation.

Lastly, I would like to acknowledge my family and friends. I am especially grateful to my parents for their continual support and encouragement.

INTRODUCTION

Most studies on the locomotion of aquatic animals have focused on fast-start responses or on performance during steady swimming (see Blake, 2004 for an extensive review; Domenici and Blake, 1997; Firth and Blake, 1991; Harper and Blake, 1990; Wardle, 1975; Webb, 1977; Webb, 1978; Weihs, 1973). Comparatively, little research has been done on the manoeuvrability of aquatic organisms — which Norberg and Rayner (1987) defined as the ability to turn in a confined space (Gerstner, 1999; Schrank et al., 1999; Walker, 2000; Webb, 1983). Yet, the majority of aquatic animals rarely swim in a steady linear fashion especially in coastal environments that are often structurally complex. Organisms in coastal environments constantly need to manoeuvre and to adjust their trajectories in the face of destabilising currents or to avoid obstacles. Manoeuvrability is also a key component of predator-prey interactions in the aquatic environment where predators are often substantially larger and faster than their prey (Howland, 1974).

In the case of marine mammals, and especially pinnipeds, the majority of kinetic studies have concentrated on measuring drag, functional design, and maximum linear speed (Domenici and Blake, 2000; English, 1976; Feldkamp, 1987b; Fish, 1993; Fish et al., 1988; Ponganis et al., 1990; Stelle et al., 2000; Williams and Kooyman, 1985). Few have considered the swimming manoeuvrability of marine mammals (Fish et al., 2003; Gerstner, 1999; Maresh et al., 2004; Schrank et al., 1999; Walker, 2000; Webb, 1983).

In a series of recent papers, Weihs (2002) and Fish (2002) discussed the direct conflict between manoeuvrability and stability in aquatic locomotion and its effect on the functional design of active aquatic organisms. By definition, a manoeuvre is a change of trajectory or velocity caused by a linear or rotational acceleration. In other words, it is a controlled instability during which the sum of all forces and moments of force acting on the centre of gravity of the animal do not equal zero. This creation of unbalanced forces is theoretically promoted by morphological characteristics, such as body flexibility or highly mobile control surfaces positioned close to the centre of gravity (Fish, 1997; Fish et al., 2003). In contrast, adaptations such as a rigid body, rigid appendages, the isolation of

the thrust-producing unit from the rest of the body, or the limited mobility of the control surfaces are all representatives of a stable design and poor manoeuvrability. Blake *et al.* (1995) show that the mean turning radius of yellowfin tuna (0.47 L), a rigid thunniform swimmer (a specialist Body and Caudal Fin — BCF — periodic swimmer, Webb, 1984), is much higher than more flexible teleosts such as the dolphinfish (0.13 L), the smallmouth bass (0.13 L), or the trout (0.18 L). However, matters are made more complex by the fact that some rigid-bodied swimmers such as the boxfish have small turning radii (Blake, 1977; Walker, 2000). The boxfish uses combined oscillations and undulation of the pectoral, dorsal and anal fins (Blake, 1977). Blake *et al.* (1995) therefore proposed that other parameters, such as decoupled propulsors (i.e. Median and Paired Fins — MPF — for slow and tight manoeuvres, and BCF motion for fast-starts), play a role in the swimming and manoeuvring performance of various species.

The turns of most animals are made up of two elements: rotation and translation (exceptions to this rule are some MPF swimmers, which can generate rotation without linear speed, e.g. the boxfish; or some species that exhibit translation without rotational speed due to a differential deflection of their fins, e.g. seahorses). The most successful individuals engaged in predator-prey interactions are typically those who maximise both turning components, i.e. perform a tight turn and maintain a high translation speed (Howland, 1974). In a recent study, Maresh *et al.* (2004) showed that bottlenose dolphins (also BCF periodic swimmers with a fairly rigid body) are capable of high manoeuvrability, as exhibited by the pinwheel turning technique (also in Nowacek, 2002). This pinwheel technique allows the animal to minimise turning radius and maximise turning rate by transforming its forward speed into rotational speed.

The relative inflexibility of such rigid organisms as the boxfish or the bottlenose dolphin theoretically impairs their manoeuvrability even though they are capable of performing tight turns. This is because the angle between the body and the incoming flow of a rotating rigid body is close to 90 degrees along the entire body length, which results in an important pressure drag around the body that opposes rotation and causes deceleration. A second outcome of having an inflexible body is that

counterbalancing moments of force are created on both sides of the dorso-ventral rotational axis, which also resists rotation (Walker, 2000). To my knowledge, no study has yet provided data to test these two theoretical assumptions in aquatic animals.

Animals must generate a force in the direction of the manoeuvre to change their trajectory using a force produced by the body itself, the control surfaces, or both. In the aquatic environment, active animals can generate this force through either a lift-based or a drag-based mechanism, both of which induce drag. This additional drag results in manoeuvring being hydrodynamically more costly than steady swimming. This conclusion is supported by Webb (1991), and Hughes and Kelly (1996) who found that a fish works harder when swimming at a given average speed in unsteady swimming than at the same speed in steady swimming.

Valuable information on the minimum amount of drag experienced by sea lions swimming at various speeds can be obtained by analyzing deceleration during passive glides. However, drag is likely to be greater during active swimming — and especially during manoeuvres — due to flippers and body movements (Stelle, 1997). Analysing the details of the pectoral and body movements and their effects on the animal's speed can thus deepen our understanding of the bioenergetics of unsteady swimming and the costs of locomotion.

Some kinematic data have been collected for otariids on swimming speeds, pectoral flipper propulsion, turning radius, turning rate, and general turning technique (English, 1976; Feldkamp, 1987a; Fish et al., 2003; Ponganis et al., 1990). They suggest that otariids have several kinematic features that enhance thrust production as well as manoeuvrability. First, their thrust production technique is based on both a lift- and a drag-based mechanism, which allows them to produce a maximum amount of thrust throughout the stroke cycle. Second, their body design is ideal for promoting instabilities (i.e., they have a highly flexible body that has a round cross-section and large mobile pectoral flippers placed close to the centre of gravity).

California sea lions are among the most manoeuvrable of marine mammals when compared to species that swim at mechanically equivalent speeds (Fish et al., 2003). However, knowledge about

the kinematics of other otariids is limited. The Steller sea lion is an ideal study animal to expand current knowledge about the manoeuvrability of otariids. Being the largest of the family, Steller sea lions experience a high value of drag and important inertial forces, both of which are likely to constrain manoeuvrability. Drag is a backwards acting force that opposes forward motion, and inertial forces tend to maintain the directionality and resist a change in trajectory while swimming. Studying detailed kinematics and morphological adaptations will provide information on how Steller sea lions manage these constraints to optimize turning capabilities and swimming velocities.

To provide data about the detailed biomechanics of an unstable body design during a manoeuvre, I repeatedly filmed 3 Steller sea lions performing 180 degree turns. Movements of the flexible body were tracked digitally throughout the manoeuvres using three markers placed along the body midline. The sequence of resulting movements was correlated with detailed speed variations and with the forces acting on the centre of gravity throughout the manoeuvres. The evaluation of acceleration (positive and negative) during the turn also provided practical information regarding the power requirements and energetics of a manoeuvring sea lion.

MATERIALS AND METHODS

All procedures and protocols involving animals were conducted under the authority of the University of British Columbia Animal Care Permit No. A04-0169.

Morphology

Morphological measurements were taken on three female Steller sea lions at the Vancouver Aquarium Marine Science Centre (Vancouver, BC, Canada). Two females were 3 year old juveniles (F00YA and F00TS — later referred to as SL1 and SL2 respectively) and the third female was a 6 year old adult (F97HA — referred to as SL3). Measurements were gathered on each animal prior to the filmed experiments. Total length was measured from the tip of the nose to the tip of the hind flippers. Standard length was taken from the tip of the nose to the base of the tail.

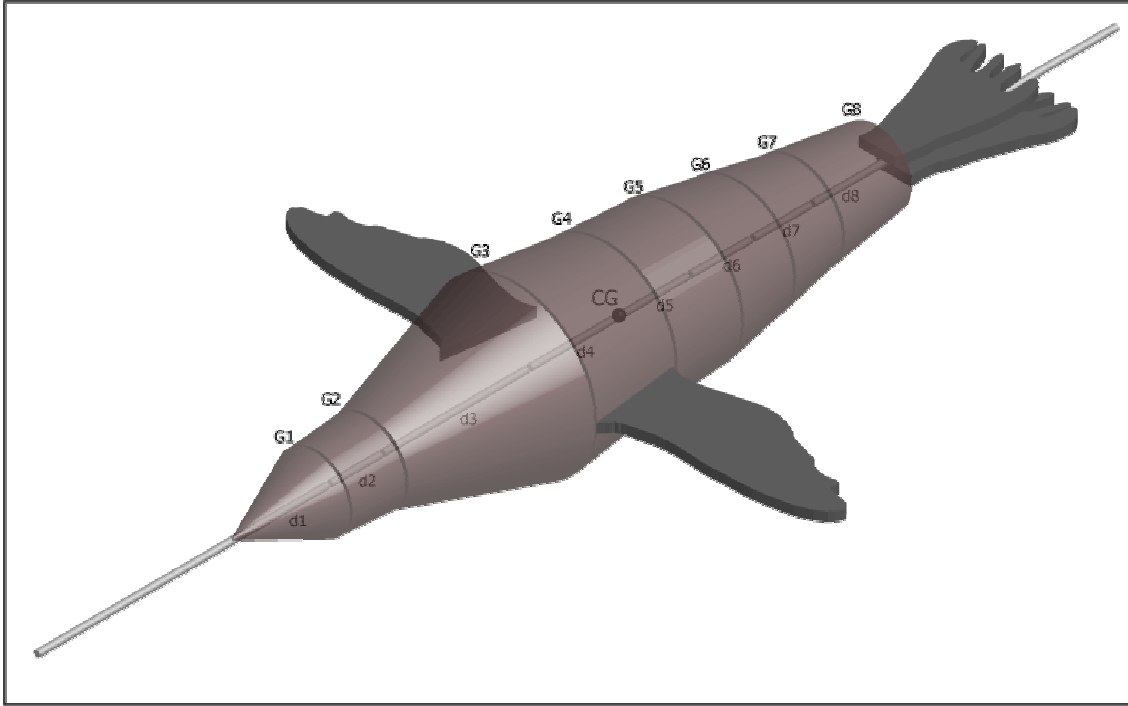


Fig. 1: 3-D representation of the body of SL3 as obtained from girth measurements. G1-G8 represent girth measurements 1 to 8 and form the base and the top of each truncated cone. Distances between each girth measurement (d1-d8) provide the height of the truncated cones. CG indicates the centre of gravity, just before the trailing edge of the pectoral flippers.

Body volume and wetted surface area were calculated as a succession of truncated cones. Eight girth measurements were taken at known intervals along the body (the ears, the neck, directly in front of the pectoral flippers, directly behind the pectoral flippers, two places along the trunk region between flippers and hips, the hips, and the position where the body and the hind flippers meet), each forming the base of a truncated cone (Fig. 1). The animals were weighed daily on a GSE scale, Model 350 (scale accuracy $\pm 0.1\text{kg}$). Body density was obtained by dividing the calculated volume (including the volume of the flippers, see below) by the mass of the animal.

The location of the centre of gravity was determined using the method of Domning and De Buffrénil (1991). In brief, an anaesthetised sea lion was placed on a flat board with the pectoral flippers lying flat against its flank. The board and sea lion were then carefully balanced in a seesaw fashion on a steel pipe. The position of the equilibrium point corresponded to the centre of mass of both the animal and the flat board together. The exact position of the animal's CG from the tip of the nose was then calculated by subtracting the effect of the board. The relative position of the CG was thus:

$$\text{Relative CG position} = \frac{\text{distance nose} - \text{CG}}{\text{standard length}} \cdot 100 .$$

The distance between the nose and the position of maximum thickness was also measured while the animal was anaesthetised and the relative position of the maximum thickness was calculated using:

$$\text{Relative max thickness position} = \frac{\text{distance nose} - \text{max thickness}}{\text{standard length}} \cdot 100 .$$

As two of the three study animals were still growing juveniles, body mass was measured daily. Additional measurements of body length and 4 girths were taken at least once a week. Fluctuations in mass were observed during the course of the study (between 5.6% and 7.6% of the body weight). I determined the possible morphological implications of this weight change by looking at the lifetime morphological data of each animal (Fig. 2). Based on the long-term relationships between weight and girths (G3, G4, G7 and G8, see Fig. 2) I determined that a girth measurement error of 3% covered the possible morphological effects of the change in mass that occurred over the course of the study.

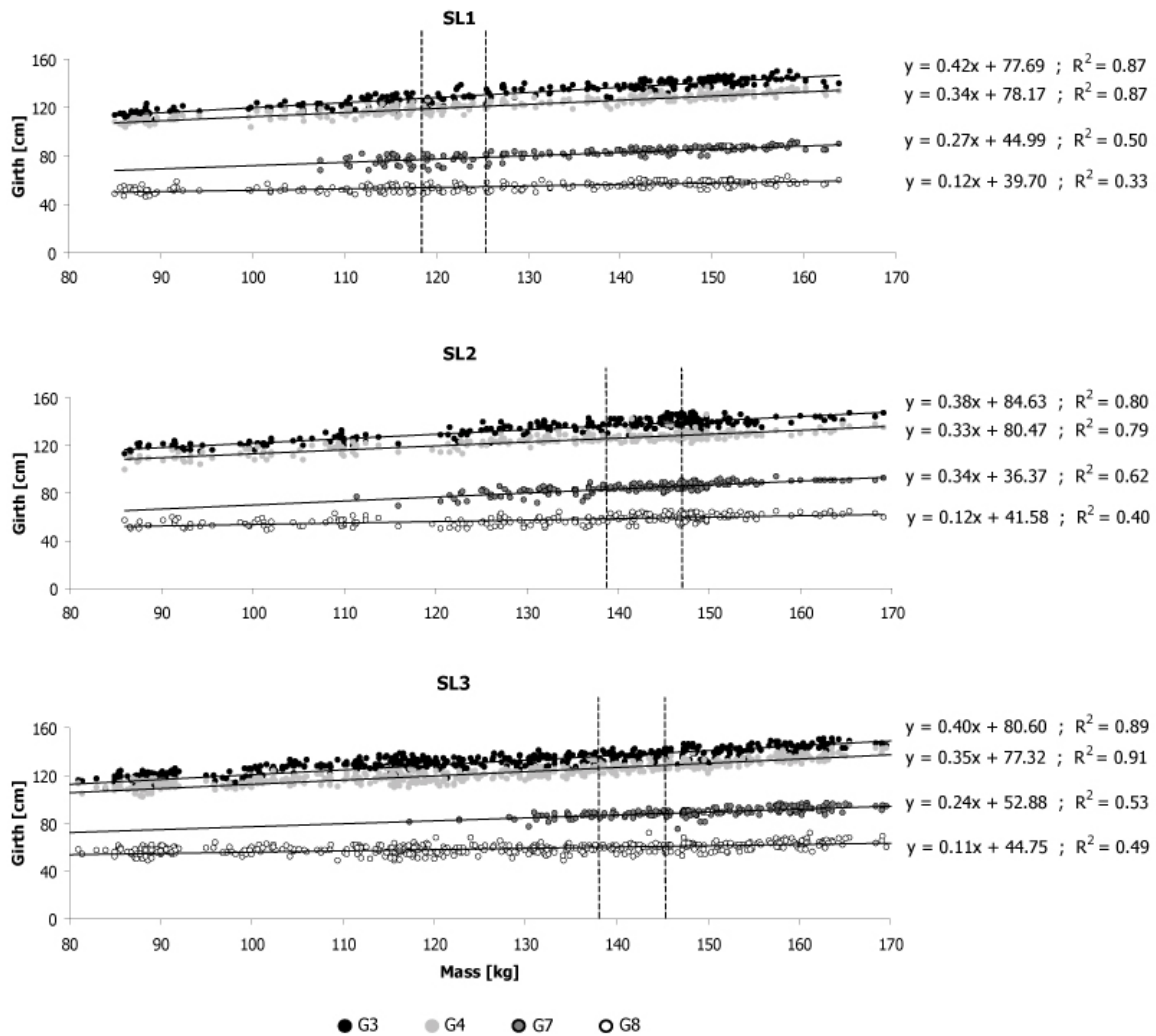


Fig. 2: Lifetime variation of 4 girth measurements as a function of body mass. Each cloud of data represents the girth of one cross-section of the body (see Fig. 1): G3 is taken just in front of the pectoral flippers; G4, just posterior to the pectoral flippers; G7 on the hipbone; and G8 on the base of the tail. The dashed lines indicate the minimum and maximum weight of each animal over the study period.

Flipper measurements were obtained via 2 different techniques. The projected surface area, length of the flipper from the insertion to the tip of the appendage and width of the flipper were taken from scaled still photographs analysed on a PC with Scion Image software (Beta version 4.0.2). Thickness measurements were obtained with a spring-joint calliper and a millimetric ruler (measurement accuracy: $\pm 0.5\text{mm}$) at 13 locations along the pectoral flipper while the animal was under anaesthetics. The 13 measurements were located as follow: 4 along the leading edge, 4 along the midline, 4 along the trailing edge, and 1 at the tip (all measurements were approximately 15cm apart). The flipper Aspect Ratio (AR) was calculated as:

$$AR = \frac{(\text{length})^2}{(\text{projected surface area})}$$

The volume of the pectoral flipper was calculated by assuming that it was equivalent to a succession of truncated, square-based pyramids (the thickness of the base of the pyramid is the average thickness of the leading and trailing edges of the flipper). These measurements were taken on one appendage only, and it was assumed that both flippers were identical. The volume of the pelvic flippers was calculated as a percentage of the volume of the pectoral flippers. This percentage was given by the ratio of the surface areas of the pelvic and pectoral flippers. These values were used in the calculation of the total volume of the animal.

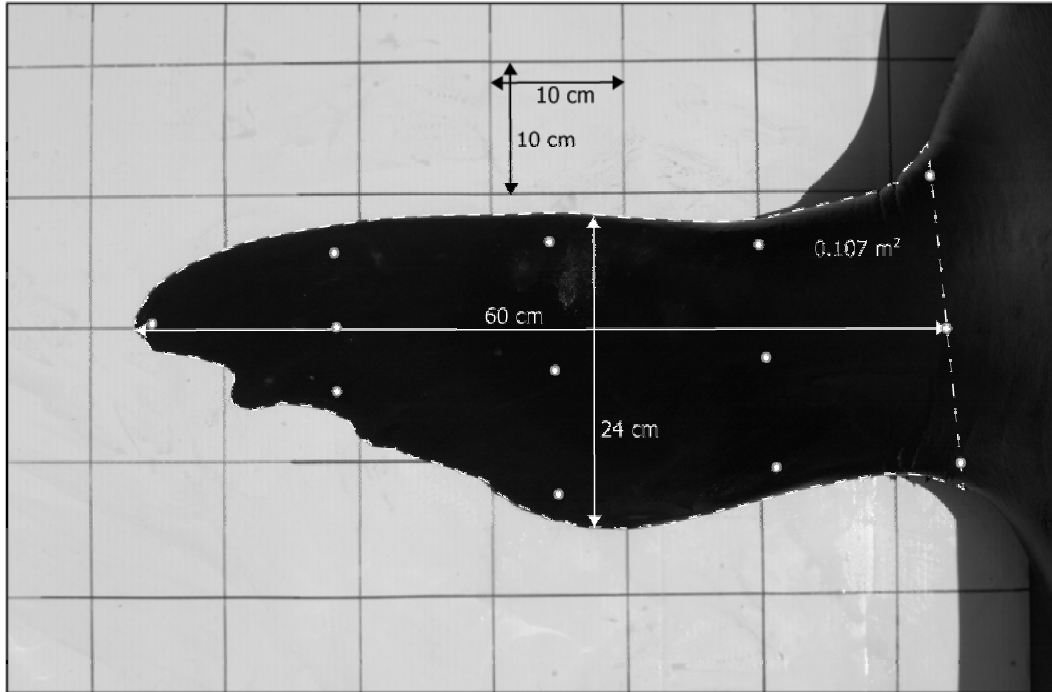


Fig. 3: On-screen morphological measurements of the left pectoral flipper of SL3. The white dots indicate points where thickness of the flipper was measured with a spring-joint calliper.

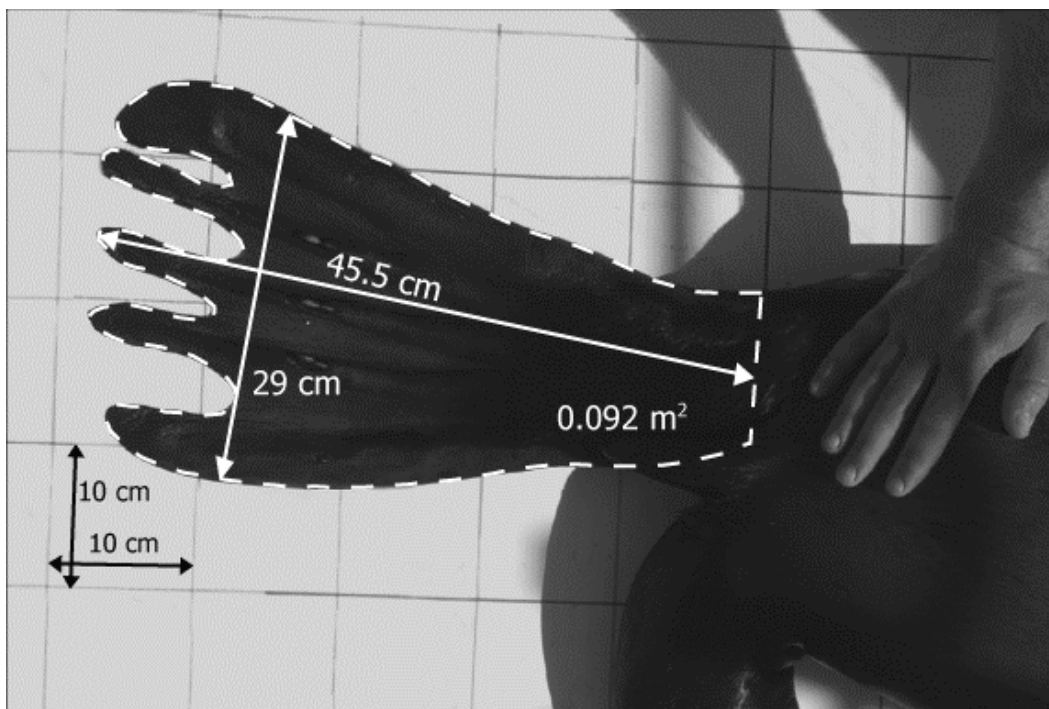


Fig. 4: On-screen morphological measurements of the left pelvic flipper of SL3. Length was measured from the base of the tail to the tip of the middle digit. Width was measured perpendicular to the flipper longitudinal axis at the base of the digital extensions.

Experimental set-up

The animals were kept in an outdoor facility with constant access to ambient, filtered seawater (Rosen and Trites, 2004). Tests were performed in a 19m long, 5m deep pool with rock and wooden haul-out areas. During the course of the study, the animals were fed predominantly Pacific herring. In addition to the daily weight measurements, morphological data (i.e. length and girths) was gathered once a week.

Data were collected from August 15th to December 3rd, 2003. Experiments occurred over a period of 11 days with SL3, 50 days with SL1, and 29 days with SL2.

The training technique used was similar to that used by Fish (2003). Using positive reinforcement, the sea lions were trained to swim back and forth between two trainers positioned at opposite ends of the test pool. As the animal approached Trainer 2, Trainer 1 would perform a recall signal (i.e. hit the surface of the water with a target pole) indicating to the animal to immediately return to Trainer 1. The animal would then execute a 180-degree turn to change its direction. Preliminary testing revealed that the longer the distance between the trainers, the lower the animal's swimming speed. Having one trainer sitting in a kayak positioned 3-5 metres from the field of view of the video camera consequently reduced this distance. Even though the distance between the two trainers varied (between 9 and 12 metres), I ensured that the animal had room for at least one complete flipper stroke before entering the field of view of the camera.

The 180-degree turns were filmed with a digital video camera (Canon GL-2) attached 5m above the water surface. The filming rate was set at 60 frames per second and the zoom setting was equivalent to a 39.5mm opening on a 35mm focal length, which corresponded to a diagonal angle of 57.42° (angle formed at the apex of the triangle defined by two opposite corners of the field of view and the focal point of the camera). To reduce flares and surface reflections, the camera was mounted with a circular polarising filter (Hoya circular polarising filter, 58mm, pitch: 0.75). A clear Plexiglas sheet (dimensions: 2.61 metres by 1.98 metres) floated on the water surface in the centre

of the field of view of the camera to eliminate visual distortions produced by the surface waves. Only the turns that occurred directly under the Plexiglas sheet were analysed.

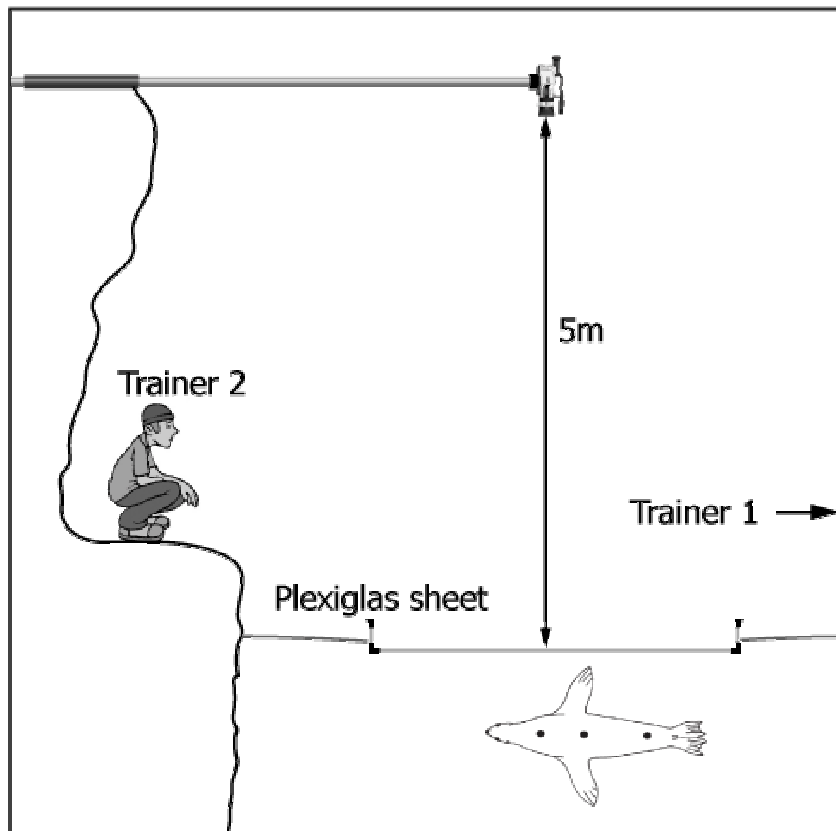


Fig. 5: Schematic of the experimental set-up.

A number of temporary marks were drawn on the fur of the test animals that could be tracked on the video images. Oil-based pastel crayons were used because the captive animals could not be marked with long-lasting paint. The dots were visible for 48 hours before having to be reapplied. However, an oil-based zinc cream was used (Desitin, Zinc Oxide 37%, Cod Liver Oil 13.5%) for one of the three test animals. This was quicker to apply but it had to be re-applied during the experiments because it faded faster while the animal was in the water. The first point was placed on the shoulder blades to represent the movements of the anterior part of the body during each manoeuvre. The second point was situated at the centre of gravity of the animal lying flat with its pectoral flipper tucked in. The third point was placed on the hipbone to represent the movements of the posterior part of the body during turns. Each visual marking was drawn 3 times around the

animal girths: on the left side, on the right side, and along the backbone. Thus a total of 9 dots (roughly 2.5 cm in diameter) were painted on each test animal.

Video analysis

During each manoeuvre, a series of 12 events were identified and classified in a time sequence to illustrate the turning technique of each animal. These 12 components were:

- 1) movement of the head inside the turn;
- 2) start of the abduction of the pectoral flippers;
- 3) start of the roll of the body;
- 4) opening of the interdigital web of the pelvic flippers;
- 5) start of the dorsal flexion;
- 6) end of the abduction of the pectoral flippers;
- 7) maximum roll;
- 8) minimum radius of curvature of the flexed body;
- 9) start of the adduction of the pectoral flippers;
- 10) body back in a straight position;
- 11) end of the adduction of the pectoral flipper;
- 12) the pelvic flippers return to a passive, gliding position.

The depth at the beginning and end of a manoeuvre occasionally differed because the motion of the animals was not limited vertically. When this happened, the turning radius as seen in 2 dimensions by the camera placed overhead (with its axis normal to the water surface) appears smaller than it really is in 3 dimensions. This was corrected using a scale that linked the size of an object on screen to its depth: i.e. a visual scale (a 2m long ruler with 10cm black and white increments) was built and filmed in the experimental set-up at various known depths. From this, a mathematical relationship was obtained that linked the two entities:

$$\text{Depth} = -0.0564 \cdot (\text{Size on screen in pixels}) + 8.633.$$

The object measured before and after each manoeuvre was the distance between the hip and the shoulder dots, which was measured digitally on scaled video images the day of the trial.

Turning radii, instantaneous speed at the start and end of a turn, average speed, acceleration, deceleration, rolling degree, and duration of the manoeuvre were all measured from the scaled video clips using Lenox Softworks' Videopoint 2.5. All manoeuvres were referenced to an on-screen origin that was positioned 16 pixels right and 16 pixels up from the bottom left corner of the image.

The positions of the three lateral dots (shoulder, CG, and hips) were manually tracked at a sampling rate of 30Hz. On most images, the painted marks covered a surface of a few pixels on screen (typically between 2 and 9 square pixels). The exact position of each mark had to be determined subsequently using the speed profiles (see below).

Instantaneous speed was calculated as:

$$U_n = \frac{P_{n+1} - P_{n-1}}{t_{n+1} - t_{n-1}},$$

where U_n is the instantaneous speed of point n (in m/s), P_{n+1} and P_{n-1} are the positions of the points directly after and before point n respectively (in m), and t_{n+1} and t_{n-1} is the time code of the points directly after and before point n respectively (in s). The speed profile was obtained by plotting instantaneous velocities over time. The speed curve was then smoothed by moving the track points a few pixels left, right, up, or down within the onscreen surface of the painted dot. This determined the exact position of the marker onscreen. To correct for the difference of depth before and after the manoeuvre, the speed calculation was modified, such as:

$$U_{n(corrected)} = \frac{U_n}{\cos \alpha},$$

where α is the angle that describes the difference of depth.

Turning radius (R) was calculated mathematically by fitting a half-circle to the curved part of the trajectories of the shoulder, the centre of gravity, and the hip using least squared regressions (i.e. three turning radii were obtained per manoeuvre). The trajectories obtained in Videopoint 2.5 were imported into S-PLUS 6.1, where the least squared regressions were performed. Once R was measured, the real turning radius was obtained by taking the depth difference into account:

$$R_{real} = \sqrt{(R_{measured})^2 + \left(\frac{\Delta D}{2}\right)^2},$$

where R is turning radius, and ΔD is the difference of depth between the entrance and exit of a manoeuvre.

Negative and positive accelerations were obtained by calculating the slope of the best fitting line through the appropriate portion of the time-speed graph (i.e. one line was fitted to the decelerating section of the graph and another was fitted to the accelerating section). These portions of the data set were identified visually.

The speed at the beginning of the turn was defined as the instantaneous speed of the animal just before the first manoeuvring movement (most of the time, a head movement and the abduction of the pectoral flippers). The speed at the end of a manoeuvre was defined as the instantaneous speed of the animal as soon as the midline of the body had regained a straight position, with the pectoral flippers adducted along the body flanks. Rolling degree could not be measured directly in degrees or radians using the one camera angle. Instead, an index of roll was used to give a sense of how much and how fast the animal turned its back into the turn before executing the manoeuvre. This 'rolling index' — tracked at 30Hz throughout the turn — was defined as the distance, normal to the body axis, between the shoulder marker and the edge of the body as seen on the top-down camera view. This distance therefore decreased with an increasing rolling degree (up to a maximum rolling degree of 180 degrees — which corresponded to a distance of 0cm).

The rolling index also provided information on how fast a sea lion rolled. It was measured between the "time of entering" (i.e. the time at which the instantaneous entering speed was measured) and the time of maximum roll (i.e. when the rolling index is minimal or, in other words, when the distance between the shoulder marker and the edge of the body — as seen from above — was minimal). The duration of a manoeuvre was defined as the time elapsed between the "time of entering" and the "time of exiting".

From the instantaneous speed data of the three markers, I obtained the resultant acceleration:

$$a_p = \frac{U_{p+1} - U_{p-1}}{t_{p+1} - t_{p-1}},$$

where a_p is the instantaneous resultant acceleration of point p (in m/s^2), U_{p+1} and U_{p-1} are the instantaneous velocities of the points directly after and before point p respectively (in m/s), and t_{p+1} and t_{p-1} is the time code of the points directly after and before point p respectively (in s).

The measurement of acceleration (and therefore force) was very sensitive to the position of the markers on each frame. I therefore fitted the position-time data with a polynomial function of the 6th degree, and calculated the second derivative of this polynomial function to obtain acceleration. This process provided the X and Y components of the acceleration vector, which were then translated and rotated to track the forward velocity vector (i.e. the velocity vector having no X component in the new referential system). Calculating the X and Y components of the acceleration vector in this new referential system provided one component parallel to the instantaneous velocity vector (tangential acceleration a_t) and one component perpendicular to the velocity vector (normal acceleration a_n). Tangential force was $F_t = m \cdot a_t$ and normal force was defined as $F_n = m \cdot a_n$.

The degree of curvature of the flexing body was quantified by calculating the radius of the circumcircle that passed through each one of the three on-screen markers. However, the degree of curvature of the body was clearly influenced by the position of the head during the turn, which was not captured by the markers located on the shoulder, CG and hips of the animal. Therefore, the position of the animal's nose was tracked using a fourth marker on 31 turns (SL1: 6; SL2: 9; SL3: 16) to provide information on the head's position and its importance in the kinematics of the turn.

ANOVA tests were performed on various parameters described above (i.e. entering speed, exiting speed, rolling time, turn duration, deceleration, acceleration, and turning radius) to determine inter-animal differences and differences between various body parts (SPSS 8.0). Results were considered significant at $P \leq 0.05$.

RESULTS

Morphology

The morphological data for each of the three sea lions is presented in Tables 1, 2, and 3, as well as Figs 1, 3, and 4. The data shown in Tables 2 and 3 were obtained prior to the first trial of each animal. The animals' weights fluctuated over the course of the study. The maximum mass change for each animal over the study period was 7.6% for SL1, 5.8% for SL2, and 5.6% for SL3. Body length showed considerably less variation with an average increase of 0.65% (range 0.22-1.43%). The highest values of the range were used to determine the uncertainties of the morphological measurements directly affected by mass variations (Table 2).

With the exception of the hipbone area (where the body is slightly dorso-ventrally compressed), the body of the Steller sea lions has a rounded cross section when in the water (personal observations). Therefore, a circular cross-section was assumed in all calculations of volume, wetted surface area, and frontal surface area.

Pectoral flippers and pelvic flippers represented 55.75% and 44.25% of the total projected flipper area respectively. The mean aspect ratio of the pectoral flippers was 3.23, and the mean aspect ratio of the pelvic flippers was 2.39.

Table 1: Mass of the three female Steller sea lions: SL1, SL2, and SL3 on the day of the filmed trials.

Animal	Age [yrs]	Birth year	Date [dd-mm-yyyy]	Mass [kg]
SL1	3	2000	12-08-2003	124.6
			15-08-2003	126.5
			18-08-2003	127.0
			22-08-2003	128.4
			13-09-2003	118.7
			15-09-2003	121.2
			19-09-2003	121.5
			03-10-2003	125.5
SL2	3	2000	30-10-2003	138.8
			05-11-2003	142.9
			06-11-2003	142.8
			07-11-2003	143.6
			11-11-2003	144.7
			12-11-2003	145.9
			25-11-2003	146.4
			27-11-2003	147.3
03-12-2003	147.3			
SL3	6	1997	03-07-2003	138.2
			28-08-2003	145.2
			29-08-2003	145.8
			30-08-2003	145.6
			31-08-2003	145.4
			02-09-2003	145.7
			07-09-2003	146.4

Table 2: Morphological data collected on three female Steller sea lions. These measurements were obtained once for each animal before their first filmed trial. Total length represents the length of the animal from the nose to the tip of the pelvic flippers. Standard length represents length to the base of the tail, and frontal surface area corresponds to the surface of the largest cross-section of the animal. Fineness ratio was calculated as: (max length)/(max breadth). The position of the centre of gravity of the animal lying stretched was determined using the technique described by Domning and De Buffrénil (1991). Total length, standard length, frontal surface area, position of maximum thickness, as well as CG position were obtained while the animal was under anaesthesia. The volume is obtained from a series of truncated cones (see Fig. 1) defined by 8 girth measurements taken at known intervals along the body of the animal. All measurements and calculations of the pectoral and pelvic flippers were obtained from digital, scaled pictures (see Figs 3 and 4). Pectoral length represents the length from the base of the pectoral flipper to its tip. Pelvic length represents the length of the pelvic flipper between the base of the tail and the tip of the middle digit. Finally, pelvic max width represents the width of the spread-out pelvic flipper right at the base of the digital extensions. Measurements were taken on one flipper only and it was assumed that the second flipper was identical. Total flipper area was therefore 2 x (pectoral flipper area + pelvic flipper area).

		SL1	SL2	SL3
Total length	[m]	2.27 ± 0.02	2.29 ± 0.02	2.26 ± 0.02
Standard length (L)	[m]	1.83 ± 0.02	1.87 ± 0.02	1.92 ± 0.02
Frontal surface area	[m ²]	0.149 ± 0.004	0.156 ± 0.004	0.167 ± 0.004
Total wetted surface area	[m ²]	2.391 ± 0.066	2.551 ± 0.061	2.481 ± 0.059
Volume	[l]	137.3 ± 10.4	154.7 ± 8.9	150.8 ± 8.4
Fineness ratio	-	5.2 ± 0.2	5.1 ± 0.2	4.9 ± 0.2
Position of max thickness	[% of L]	44.3	42.8	45.8
CG position	[% of L]	57.4	55.6	51.6
Pectoral flipper area	[m ²]	0.104	0.115	0.107
Pectoral length	[m]	0.58	0.60	0.60
Pectoral max width	[m]	0.23	0.24	0.24
Pectoral aspect ratio	-	3.23	3.13	3.32
Pelvic flipper area	[m ²]	0.085	0.082	0.092
Pelvic length	[m]	0.45	0.46	0.46
Pelvic max width	[m]	0.28	0.25	0.29
Pelvic aspect ratio	-	2.38	2.53	2.26
Total flipper area	[m ²]	0.378	0.394	0.396

Kinematics

A total of 419 turns were filmed from August 15th to December 3rd, 2003. All turns were partially unpowered manoeuvres performed with a non-zero initial speed (a manoeuvre starting from a resting position was never observed). In all 419 events, the three animals used the same general turning technique to perform the 180-degree turns. Some kinematic parameters fluctuated between turns, such as the rolling degrees, the degrees of abduction (movement away from the midline of the body — Fish et al., 2003) of the pectoral flippers, and the dorsal arching of the backbone, etc. The animals were never observed performing a ventrally induced turn. The turning technique observed was in all regards comparable to the turning technique described by Fish *et al.* (2003) for the California sea lion. Table 3 presents the sequence of movements taking place during the manoeuvre and divides the technique into 6 main events (or series of events).

Before performing the turning sequence, the animal glided horizontally with its dorsal side towards the surface. The plantar face of the pectoral flippers was applied against the ventro-lateral side of the animal while gliding, and the pelvic flippers were contracted and held together with their plantar faces in contact. This position minimised the inter-digital web of the pelvic flippers. Upon entering the turn, the animal performed three movements: 1) the head was oriented and extended towards the inside of the turn, 2) the pectoral flippers were abducted and 3) the animal rolled to orient its back inside the turn (Fig. 6.1). The sequence of these three events varied from turn to turn and they were often performed simultaneously.

The movement of the pectoral flippers was as follows. From their gliding position, the sea lions rotated their flippers outwards and brought them away from the midline of their bodies (abduction, Figs 6.2 and 6.3). At the end of the abduction, the pectoral flippers were approximately perpendicular to the midline of the body and remained stationary until the anterior part of the body (head, neck, and torso) started to exit the turn (Fig. 6.4). During the curved part of the trajectory, the body was extended and arched dorsally in a U-shape position (Figs 6.4 and 6.5). The inter-digital web of the pelvic flippers was then extended (thus increasing their surface area) with the

ventral sides facing the outside of the turn. As the anterior body started to regain a straight position, the animal performed a pectoral flipper stroke and accelerated out of the turn (Figs 6.5 and 6.6). Finally, the pectoral flippers previously held away from the body's midline were brought back along the animal's ventro-lateral surface (i.e. adduction).

The stroke movement of the pectoral flippers was oriented downwards and backwards, and the front edges of the flippers were rotated inwards to reposition the plantar face of the pectoral flippers against the body of the animal. This motion was composed of two phases as described by Feldkamp (1987a): 1) the power phase (forceful dorso-ventral adduction, which ends in a full extension of the pectoral flippers below the body) and 2) the paddle phase (flippers oriented 'broadside to the flow' and brought backwards and upwards towards the body).

The midline of the body of the animal regained a straight position before the end of the pectoral flipper stroke. As the power phase was performed, the body rolled back to reorient the dorsal surface up, the head regained its straightforward orientation, and the neck remained extended. Lastly, the pelvic flippers were slowly rotated and brought back together in the gliding position described above (Fig. 6.6). Sometimes the animals did not roll back completely and remained at an angle as they glided out of the turn.

The trajectory of the nose of the animal differed from the rest of the body. While the trajectory of the shoulder, CG and hips were smooth (i.e. a linear glide into the turn, followed circular or elliptical turn, followed by a linear exit), the trajectory of the nose was more irregular. First, it was displaced and extended into the turn as the animal entered the manoeuvre (as described above), which resulted in an angular trajectory. Second, while the animal re-accelerated at the end of the turn, the trajectory of the nose did not follow the general direction of the rest of the body. Instead the nose appeared to initially follow a path leading towards the inside of the turn before changing its course and taking the direction followed by the rest of the body (Fig. 10). This change of trajectory corresponded with the onset of the adduction of the pectoral flippers.

The radius of the minimum circumcircle that passes through each body marker, including the nose, was measured in 31 turns. This radius, which measured the degree of dorsal curvature during the turn, ranged from 0.27L (i.e. expressed relative to the animal's body length — L) to 0.39L with an average of 0.32L (which corresponds to a range of 0.51m to 0.69m with an average of 0.6m). The radii of the 31 turns in which body curvature was measured varied between 0.17L and 0.36L with an average of 0.27L (which corresponds to a range of 0.32m to 0.64m with an average of 0.5m). Fig. 7 illustrates the relationship between the relative turning radius and the relative dorsal curvature. The larger the turning radius, the straighter the body (linear regression, $F_{30} = 18.27$, $p < 0.001$).

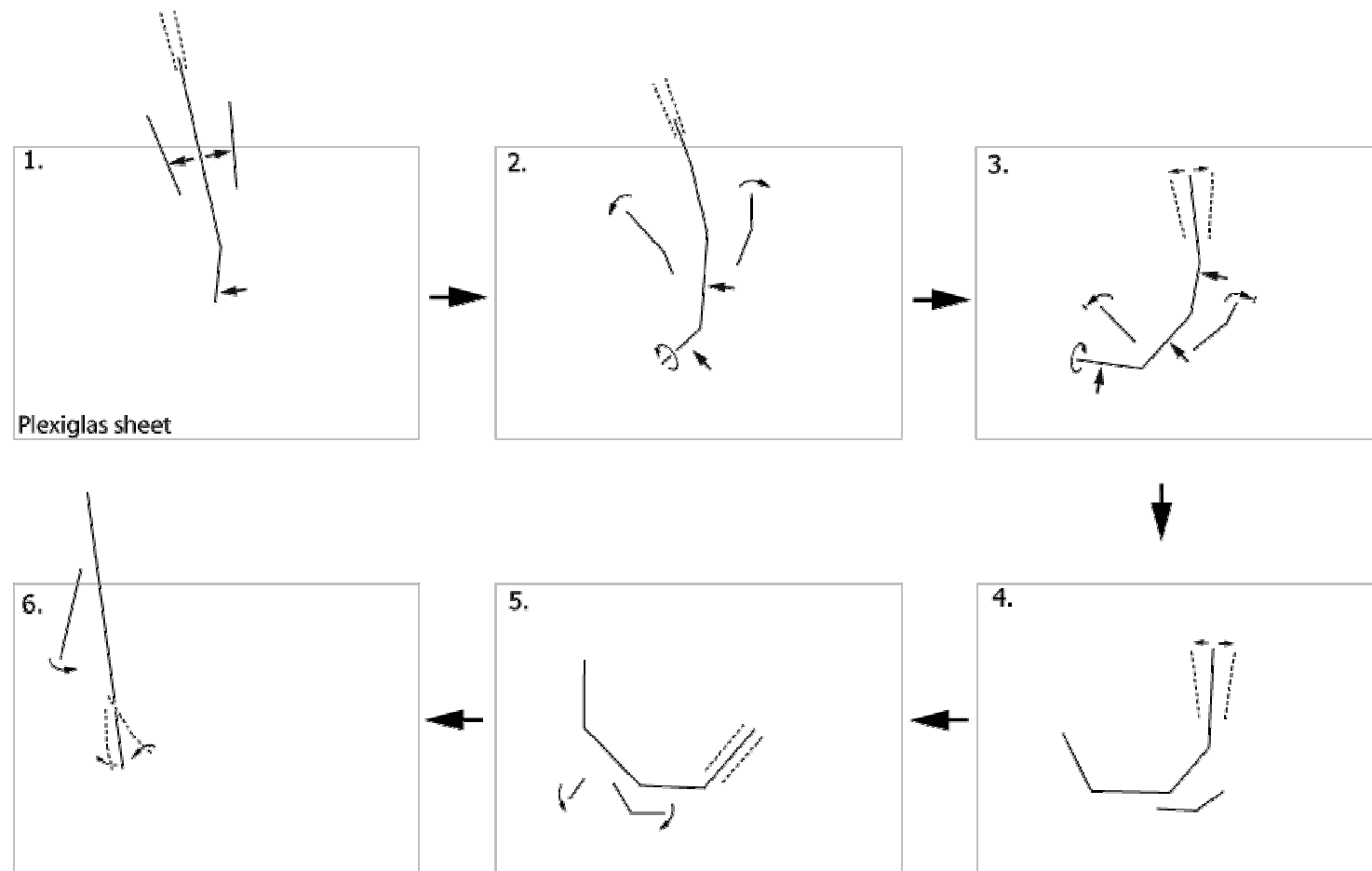


Fig. 6: Sequence of movements based on turn H128 performed by SL3. Arrows indicate the principal movements of the animal on each frame. 1. The head is oriented towards the inside of the turn and the pectoral flippers are abducted. 2. The body starts flexing dorsally and rolls. 3. The body flexion continues, the abduction of the pectoral flippers reaches an end, the body rolls, and the interdigital web of the pelvic flippers starts to unfold. 4. The roll has stopped, the body is maximally arched dorsally, the digits of the pelvic flipper open. 5. As the body regains a straight position, the pectoral flippers are adducted, the interdigital web of pelvic flippers is spread out. 6. The body regains a straight position, the pectoral flippers reach the last stage of the power stroke, and the pelvic flippers return to their gliding position.

Table 3: Sequence of movements performed by SL3 during a 180 degrees turn. Each row corresponds to a turn. The numbers between 1 and 12 in the tables describe the sequence of movements. When several actions take place at the same time, they get the same number and are highlighted in light or dark grey. "NA" signifies that a movement happened out of the field of view of the camera or that it could not be identified clearly. In that case, it is ignored from the sequence. The vertical blanks delimit shorter sequences (of 2 or 3 movements) that are repeatedly distinct from the rest of the sequence. A dashed line in the header between two sections indicates that these two sections tend to be distinct but not always. H_1 : movement of the head inside the turn; Ab_0 : start of the abduction of the pectoral flippers; R_0 : start of the roll of the body; P_{start} : opening of the interdigital web of the pelvic flippers; F_{start} : start of the dorsal flexion; Ab_1 : end of the abduction of the pectoral flippers; R_{max} : maximum roll; F_{max} : minimum radius of curvature of the flexed body; Ad_0 : start of the adduction of the pectoral flippers; F_{end} : body back in a straight position; Ad_1 : end of the adduction of the pectoral flipper; P_{end} : the plantar surfaces of the pelvic flippers are back in contact, and the inter-digital web closes gradually afterwards.

Turn	H_1	Ab_0	R_0	P_{start}	F_{start}	Ab_1	R_{max}	F_{max}	Ad_0	F_{end}	Ad_1	P_{end}
H68	2	1	3	4	5	6	7	9	8	10	10	11
H71	1	1	2	3	3	4	5	6	6	7	8	9
H73	1	1	2	NA	3	4	5	6	6	7	7	8
H74	1	1	2	NA	3	4	5	7	6	8	9	10
H75	1	1	2	NA	3	4	5	7	6	8	8	9
H77	1	1	2	4	3	5	6	7	7	8	9	10
H78	1	1	2	4	3	5	6	7	7	8	8	9
H84	1	1	2	4	3	5	6	7	7	8	9	10
H89	1	1	2	4	3	5	5	7	6	8	8	9
H92	1	1	2	4	3	5	6	7	7	8	9	10
H93	1	1	2	NA	3	4	5	6	6	7	7	8
H95	1	1	2	3	3	4	4	6	5	7	7	8
H96	1	1	2	NA	2	3	3	4	5	6	6	7
H97	1	1	1	3	2	4	5	6	6	7	7	8
H98	1	1	1	2	2	3	3	5	4	6	6	7
H99	1	1	2	3	4	5	6	7	7	8	9	10
H101	1	1	2	3	2	4	5	6	6	7	8	9
H103	1	1	2	4	3	5	5	6	6	7	8	9
H104	3	1	2	4	5	6	6	7	7	8	8	9
H105	1	1	2	3	3	4	4	5	5	6	7	8
H106	1	1	2	3	4	5	5	6	6	7	8	9
H107	2	1	3	NA	4	5	5	6	6	7	7	8
H108	1	2	3	4	4	5	5	6	6	7	8	9
H109	1	NA	2	NA	2	3	4	5	5	6	7	8
H110	1	1	2	NA	3	4	5	6	6	7	8	9
H113	1	1	2	3	3	4	5	7	6	8	9	10
H114	1	NA	2	NA	3	4	5	6	6	7	8	9
H115	1	1	2	4	3	5	6	7	7	8	9	10
H116	2	1	3	4	4	5	6	8	7	9	10	11
H117	1	1	2	NA	3	4	5	6	6	7	8	9
H128	1	1	2	4	3	5	6	7	7	8	9	10

Table 3 (continued): Sequence of movements performed by SL2.

Turn	H ₁	Ab ₀	R ₀	P _{start}	F _{start}	Ab ₁	R _{max}	F _{max}	Ad ₀	F _{end}	Ad ₁	P _{end}
T007	1	2	3	NA	4	5	NA	7	6	8	9	10
T012	1	NA	2	NA	3	4	5	6	7	8	8	NA
T080	1	2	2	NA	3	4	4	6	5	7	7	8
T081	1	1	1	NA	2	3	3	5	4	6	6	7
T108	2	1	1	NA	3	4	5	7	6	8	8	9
T109	2	1	1	NA	3	4	5	7	6	8	8	9
T111	3	1	2	4	5	6	7	9	8	10	10	11
T112	2	1	1	NA	3	4	5	7	6	8	NA	9
T113	1	1	2	NA	3	4	5	7	6	8	8	9
T114	3	1	2	6	4	5	7	9	8	10	10	11
T115	3	1	2	5	4	6	6	8	7	9	9	10
T116	1	1	2	4	3	5	5	7	6	8	9	10
T117	2	1	2	5	3	4	6	8	7	9	10	11
T118	1	1	1	3	2	4	4	6	5	7	8	9
T120	1	1	1	3	2	4	4	6	5	7	8	9
T122	2	1	1	3	3	4	4	6	5	7	8	9
T123	2	1	1	4	3	5	5	7	6	8	8	9
T124	2	1	1	4	3	5	5	7	6	8	9	10
T125	1	1	1	3	2	4	4	6	5	7	8	9
T126	2	1	1	4	3	5	6	7	7	8	9	10
T127	2	1	1	4	3	5	5	6	6	7	8	9
T129	2	1	1	4	3	5	5	7	6	8	8	9
T130	2	1	1	4	3	5	5	7	6	8	8	9
T131	2	1	1	NA	3	4	4	5	5	6	7	8
T132	2	1	1	NA	3	4	5	7	6	8	9	10
T133	2	1	1	3	3	4	5	7	6	8	9	10
T134	1	1	1	NA	2	3	3	5	4	6	7	8
T136	1	1	1	2	2	3	3	5	4	6	7	8
T138	3	1	2	4	4	5	5	7	6	8	9	10
T139	2	1	1	4	3	5	5	7	6	8	9	10

Table 3 (continued): Sequence of movements performed by SL1.

Turn	H ₁	Ab ₀	R ₀	P _{start}	F _{start}	Ab ₁	R _{max}	F _{max}	Ad ₀	F _{end}	Ad ₁	P _{end}
Y005	1	1	2	3	3	4	5	6	7	8	9	10
Y006	1	1	2	NA	3	4	5	6	7	8	8	9
Y063	1	1	2	3	3	4	5	6	7	8	8	9
Y064	1	NA	2	3	4	5	6	7	8		10	11
Y066	1	1	1	NA	2	3	3	5	4	6	6	7
Y067	1	1	2	NA	3	4	5	6	6	7	8	9
Y068	1	1	1	2	2	3	4	5	5	6	7	8
Y069	2	1	1	4	3	5	6	7	8	9	10	11
Y070	1	NA	2	4	3	5	5	7	6	8	8	9
Y072	2	1	1	4	3	5	NA	6	6	7	7	8
Y073	2	1	3	5	4	5	6	7	8	9	10	11
Y074	1	1	2	4	3	5	6	7	7	8	9	10
Y076	1	2	2	4	3	5	5	6	6	7	8	9
Y095	3	1	2	4	4	5	6	7	8	9	10	11
Y096	3	1	2	4	4	5	5	6	6	7	8	9
Y097	2	1	2	3	3	4	4	5	5	6	7	8
Y099	1	NA	1	3	2	4	4	5	5	6	7	8
Y100	1	NA	1	NA	2	3	3	4	4	5	6	7
Y101	1	1	1	NA	2	3	3	4	4	5	6	7
Y102	2	1	3	5	4	6	6	8	7	9	10	11
Y103	1	NA	1	NA	2	3	3	4	4	5	6	7
Y104	2	1	1	4	3	5	5	6	6	7	7	8
Y117	2	1	2	3	3	4	4	5	5	6	NA	7

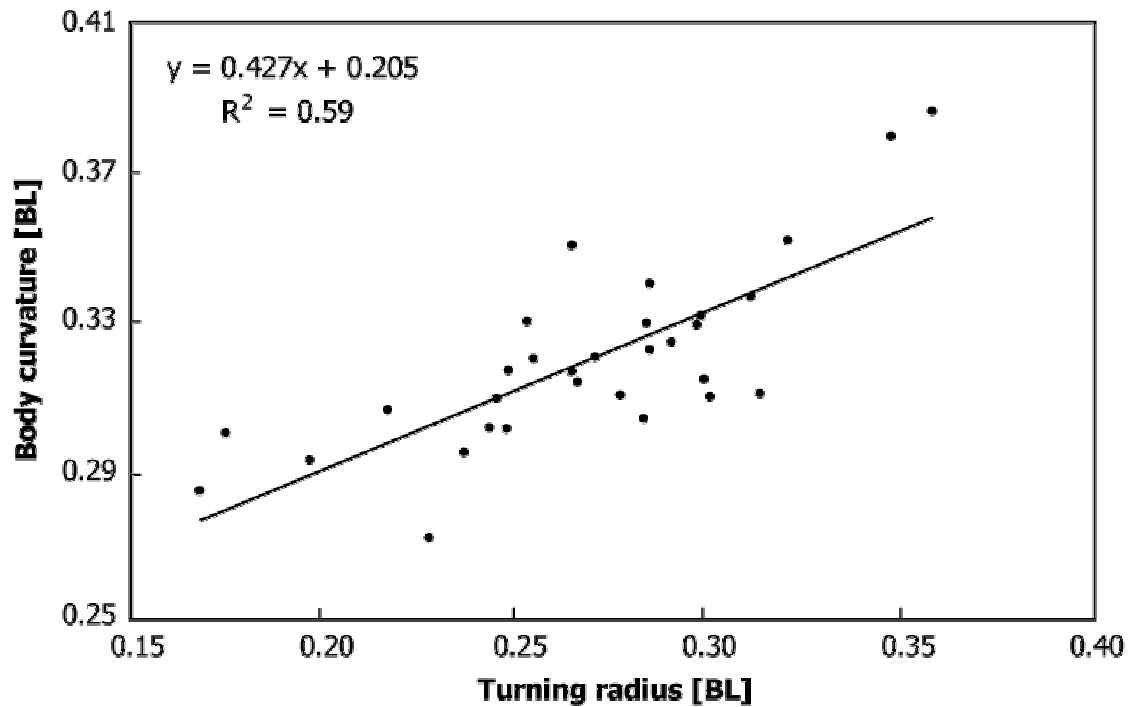


Fig. 7: Relationship between turning radius and the degree of body curvature of three Steller sea lions performing a 180 degrees turn. 31 turns are represented here. Body curvature is expressed as the radius of the circumcircle that passes through the 4 body markers: nose, shoulders, CG, and hips. All measurements are expressed relative to each animal's body length to compensate for size differences.

Kinetics

Out of the 419 turns that were filmed with the 3 test animals, 195 occurred directly under the Plexiglas sheet and were kept for further analysis. In each analysed turn, I measured turning radius, speed, angular speed, acceleration, slippage, rolling time, and manoeuvring time (64 turns for SL1, 70 for SL2, and 61 for SL3).

The turning sequence was performed in 1.65 ± 0.17 s for SL1, 1.74 ± 0.20 s for SL2, and 1.32 ± 0.13 s for SL3. These differences in turning duration were significant among all animals (one-way ANOVA; $F_2 = 80.2$, $p < 0.0001$). Inter-animal variations were observed on all measured parameters, except for the deceleration of the CG for which data were often missing because the abducted pectoral flippers covered the marker (Table 4).

The instantaneous speed data plotted against time produced a typical V-shaped curve in all turns recorded (see Fig. 8). The speed of the animals while gliding before the first movement of the turn was constant or slightly decreasing. This plateau was followed by a period of deceleration, which corresponded to the start of the turning movements (i.e. movement of the head inside the turn; start of the abduction of the pectoral flippers; start of the roll of the body). The deceleration of the centre of gravity stopped at or after the time of minimum roll, before the start of the flipper adduction. Immediately following this period of deceleration, the speed reached a minimum for a short duration before increasing again. The animal started accelerating just prior to or at the onset of the flipper adduction. Just before the end of the flipper stroke, the speed once again attained a plateau of constant or slightly decreasing speed. At this point in time, the midline of the body had not yet regained a fully straight position.

Within a turn, the speed profiles of the different body parts showed some temporal variations. The anterior part of the body (represented by the shoulder marker) decelerated faster than the middle and posterior parts (represented by CG and the hip markers respectively) (Table 4 and Fig. 9). The overall range of deceleration of the shoulder marker was from -0.27m/s^2 to -5.18m/s^2 with an average -2.19m/s^2 (± 0.84); the CG ranged from -0.39m/s^2 to -4.37m/s^2 with an average of -

1.48m/s² (\pm 0.89); the hips ranged from -0.25m/s² to -3.63m/s² with an average of -1.64m/s² (\pm 0.79) (Table 4).

Minimum speed was attained slightly before the middle of the 180 degrees trajectory of each marker. Consequently, the shoulders were the first to attain minimum speed, closely followed by the CG, which was followed by the hips. As the animal exited the turn, the shoulders and the CG re-accelerated at a similar rate, while the acceleration of the hips was considerably higher. The range of acceleration of the shoulder marker was from 0.48m/s² to 6.66m/s² with an average 3.29m/s² (\pm 1.18); the CG ranged from 0.41m/s² to 6.56m/s² with an average of 3.00m/s² (\pm 1.22); the hips ranged from 0.57m/s² to 11.98m/s² with an average of 5.00m/s² (\pm 2.26) (Table 4). As noted above, the instantaneous speed of the three markers reached a common plateau at the end of the turn.

During the turn, one component of the acceleration vector was parallel to the velocity vector (tangential acceleration) and the other was perpendicular to it (normal acceleration). Each component behaved differently (Fig. 9) and followed the temporal variations of the body parts.

The polynomial curve describing tangential acceleration closely followed the variations in the speed profile. As the animal glided before entering the manoeuvre, the value of tangential acceleration was slightly negative and close to zero. As the animal rolled into the turn and abducted its pectoral flippers, the tangential acceleration of the shoulders and CG further decreased until it reached a minimum approximately when the pectoral flippers attained their full abducted position. It then came back to zero when the speeds of both body parts reached their minimum. As speed increased, the tangential acceleration became positive and reached a maximum partway through the pectoral flipper stroke before coming back close to a nil — or slightly negative — value as the animal glided out of the turn. The hips started decelerating later, when the body started bending and the trajectory of the hips deviated from the trajectory of the other two markers. The onset of the hips deceleration corresponded to the movements of the pelvic flippers. It remained negative through the first half of the manoeuvre and reaccelerated abruptly as the hips trajectory “cut through” the other

trajectories and the body of the animal straightened. The maximum tangential acceleration of the hips was reached just before the end of the power phase. The tangential acceleration of all three markers peaked after the curved portion of their respective trajectory.

The normal acceleration had a different profile than the tangential acceleration. During the linear glide preceding the manoeuvre, the normal acceleration of the shoulder and centre of gravity was close to zero. It then increased when the animal oriented its head into the turn, started rolling and abducting the pectoral flippers, and reached a maximum just after the start of the power phase. This corresponded to a point in the manoeuvre that was slightly after the middle of the 180 degrees turn. Finally, normal acceleration of the shoulder and centre of gravity quickly came back to a nil value at the end of the power phase. The normal acceleration of the hips started at the beginning of the dorsal flexion of the body and reached its maximum halfway through the power phase. It came back to a zero value as the body regained a straight position. As with tangential acceleration, normal acceleration followed the temporal variations of the different body parts (i.e. the shoulders reached their maximum value first, followed by the CG, and then the hips).

The maximum value of normal acceleration was systematically greater than the maximum value of tangential acceleration for all three animals and all three markers. Furthermore, the maximum normal acceleration always preceded the maximum of tangential acceleration for each marker (Fig. 9).

At the beginning and end of the profiles, the acceleration curves occasionally "overshot" creating seemingly another maximum or minimum. This was an artefact of the calculation technique and depended on the shape of the 6th degree polynomial fitted to the position data (for which I took the second derivative).

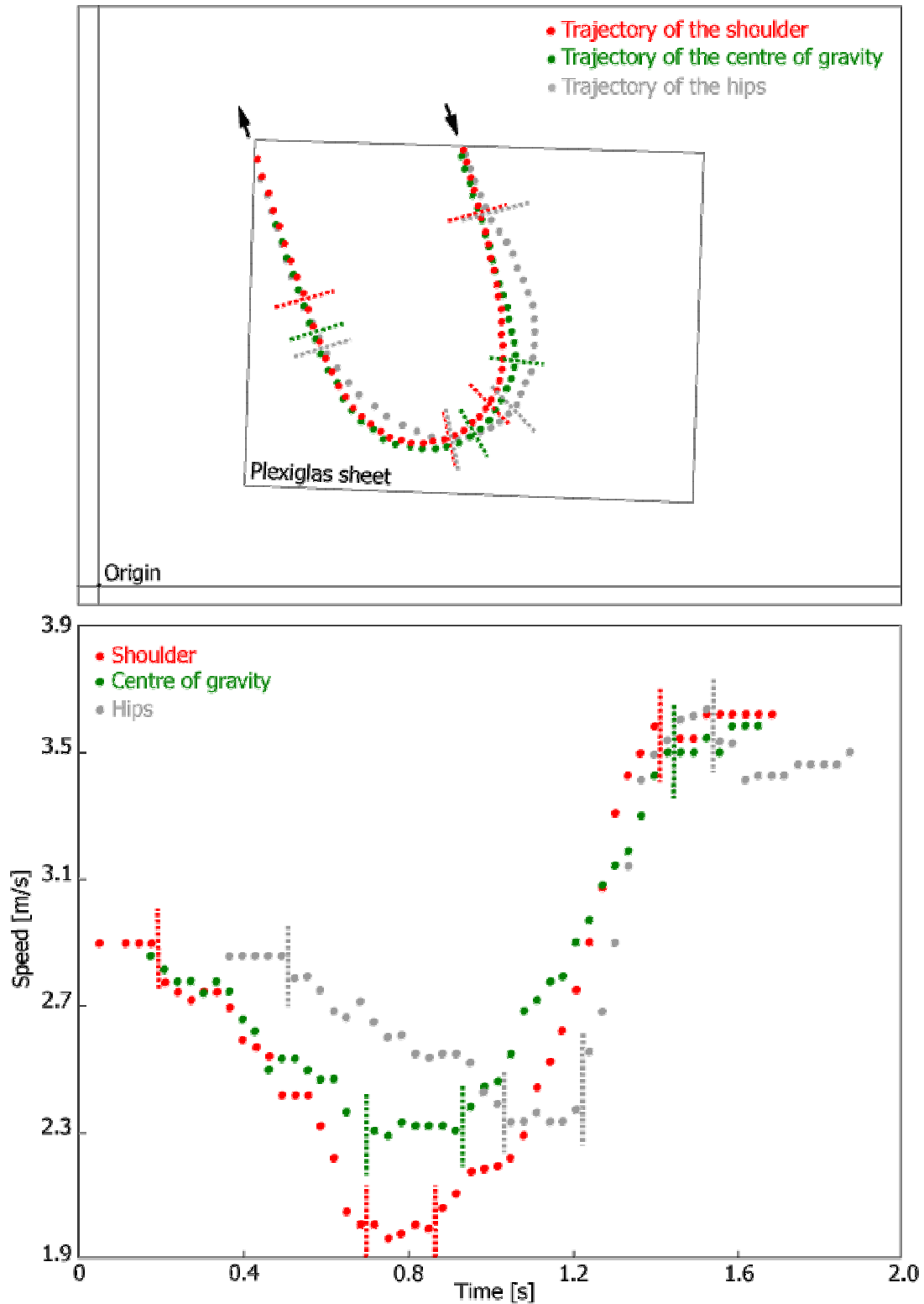


Fig. 8: Typical trajectory and speed profile of the shoulder, centre of gravity, and hips markers of a Steller sea lion performing a 180 degree turn. The dashed lines delimit the bouts of constant speed, from the bouts of deceleration and acceleration on both charts.

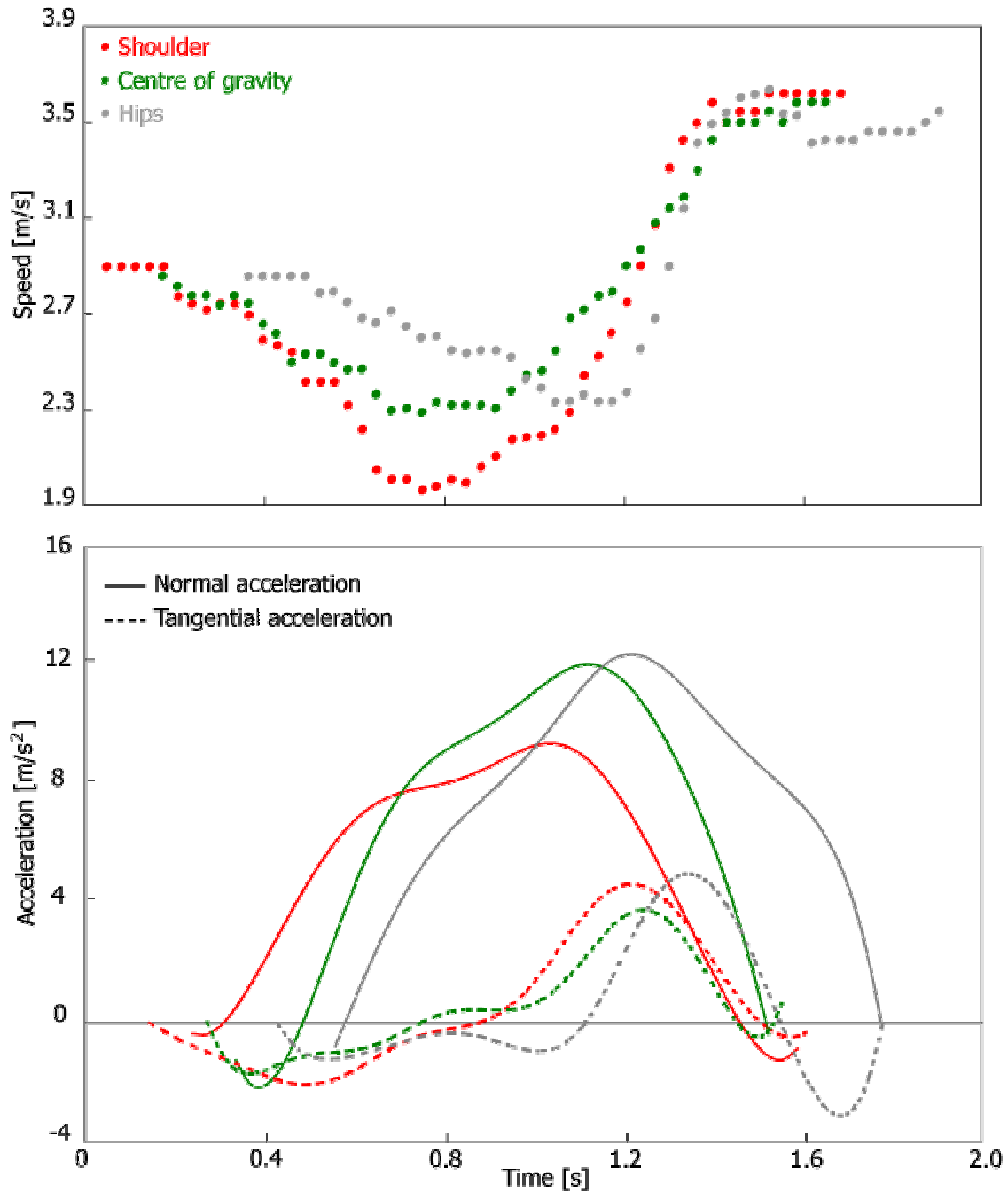


Fig. 9: Tangential and normal acceleration profiles of the shoulder, the centre of gravity, and hips markers of a Steller sea lion performing a 180 degree turn in correlation with its swimming speed. The dashed lines represent tangential acceleration and the plain lines are normal acceleration.

Table 4: Mean kinetic parameters for the SL3, SL2, and SL1. The different letters and grey tones (white, grey, dark grey) represent a significant difference between each animal at $\alpha=0.05$.

	SL1	SL2	SL3
In speed [m/s]	2.69 ^a	2.93 ^b	2.92 ^b
Out speed [m/s]	3.22 ^b	3.08 ^b	3.77 ^a
Rolling time [s]	0.76 ^b	0.74 ^b	0.64 ^a
Turn duration [s]	1.65 ^c	1.74 ^b	1.32 ^a
Turning radii [BLs]			
Shoulders	0.32 ^b	0.31 ^b	0.26 ^a
CG	0.32 ^b	0.30 ^b	0.27 ^a
Hips	0.33 ^b	0.33 ^b	0.26 ^a
Deceleration [m/s²]			
Shoulders	-1.75 ^a	-2.40 ^b	-2.43 ^b
CG	-1.31	-1.65	-1.48
Hips	-1.20 ^a	-1.84 ^b	-1.89 ^b
Acceleration [m/s²]			
Shoulders	2.50 ^c	3.39 ^b	3.96 ^a
CG	2.70 ^b	3.01 ^{a,b}	3.29 ^a
Hips	4.11 ^b	3.86 ^b	7.12 ^a

DISCUSSION

Morphology

A series of recent articles have illustrated the conflict between stability and manoeuvrability in active, mobile individuals (Fish, 1997; Fish, 2002; Fish et al., 2003; Weihs, 2002). Stability, by definition, is a property of the body that creates forces that restore its original condition when disturbed from a condition of equilibrium. In contrast, manoeuvrability is the capacity to rapidly change direction, which means quickly creating and maintaining highly unbalanced forces.

Stability is advantageous when an individual is constantly and steadily moving for an extended period of time, e.g. during migration, or during trips to foraging grounds. In these circumstances, the individual tries to optimise its energetic expenditures in relation to distance covered in order to reach its destination as cost-effectively as possible. To do so, it makes use of structures that decrease the energetic cost of steady locomotion, such as keels, rigid dorsal fins, and/or lateral compression of the body. These morphological characteristics resist roll and side to side movements, which otherwise would have to be controlled by muscular activity and would induce costs. Also, control surfaces located far from, and posterior to, the centre of gravity (CG) possess more leverage to correct for unnecessary and 'wasteful' movements. Other adaptations that minimise drag and maximize thrust production include reduced motion of the control surfaces, anterior placement of the centre of gravity, reduced flexibility of the body, isolation of the thrust producing unit from the rest of the body, and a lunate caudal fin with a high aspect ratio (large span and relatively small cord) (Blake, 2004; Fish, 1997; Fish, 2002; Fish et al., 2003).

In contrast to stability, manoeuvrability is beneficial when escaping a fast predator or when trying to capture an elusive prey (Howland, 1974). In these situations, energy conservation is less crucial than kinematic performance, because a) being caught by a predator is not an option and b) predatory success depends on the predator's ability to out-maneuvre its prey.

Steller sea lions (and otariids in general) display morphological characteristics of a very unstable body design. They have highly mobile control surfaces placed at their centres of gravity, rounded cross-sections (with the exception of the heads and the hips that are both slightly dorso-ventrally compressed), and very flexible bodies. The centre of gravity is positioned past the middle of the body (Table 2), slightly anterior to the insertion of the trailing edge of the pectoral flippers. These morphological features contrast markedly with the list of characteristics associated with stability presented above.

An unstable body design likely provides a number of ecological advantages for Steller sea lions. Domenici (2003) argues that the body design of an organism is highly influenced by their environment and life history traits (e.g. thunniforms, such as tunas, inhabit pelagic marine habitat and have one of the most stable functional design — Blake, 2004). Steller sea lions, on the other hand, are amphibious creatures that spend a substantial amount of time on land (particularly during the breeding season) and, when in the water, are mostly found from nearshore to the edge of the continental shelf (Loughlin et al., 1987; National Marine Fisheries Service, 1992). Strong and mobile pectoral flippers are an advantage on land because they support the animal's weight and allow greater mobility. Otariids are capable of agile quadrupedal locomotion on land (English, 1976). In comparison, phocids that have less developed pectoral flippers and swim using their pelvic flippers and body oscillations, are awkward and slow on land. Sea lions use their on-land agility to reproduce, rest, and escape from marine predators. More specifically, male sea lions are highly territorial during the breeding season and use their terrestrial mobility to establish territories and fight-off competitors. Their dorsal flexibility allows them to keep their torso and head in an upright position to watch over territories. Finally, Steller sea lions use their mobility on land to climb rocks out of reach of marine predators and find areas sheltered from storms.

The unstable body design of Steller sea lions is also advantageous in the aquatic environment. Steller sea lions are opportunistic predators that forage on a wide variety of prey species without a clear preference for one particular kind (Riedman, 1990; Sinclair and Zeppelin, 2002). Prey species

range across several taxa from pelagic to benthic, and from gregarious to individualistic. Merrick *et al.* (1997) classified the diet of the Steller sea lions in Alaska as: gadids (i.e. walleye pollock, Pacific cod, and Pacific hake); Pacific salmon; small schooling fish (i.e. capelin, Pacific herring, eulachon, and Pacific sand lance); flatfish (i.e. arrowtooth flounder and rock sole); other demersal fish (i.e. sculpins, rockfish, Stichaeidae, skates, sharks, and lamprey); Atka mackerel; and cephalopods (i.e. squid and octopus). These prey species use a wide variety of antipredator techniques, such as schooling and confusion techniques, cryptic behaviours, use of natural covers (i.e. kelp beds and rocky ocean floor), etc. For an active predator such as the sea lion, predatory success depends on the ability to come within striking distance of the prey and to maintain this distance long enough to launch a strike (normally a rapid neck extension followed by a bite, which occasionally involves suction of water — personal observations). The extent to which Steller sea lions use collective foraging techniques is not clear, but it appears that sea lions typically capture one prey at a time and have to ingest it before capturing the next one (personal observations). Thus the final bout of all predatory strikes is a one-on-one interaction between the sea lion and its prey. It is during this crucial final approach towards a much smaller and more manoeuvrable prey item that manoeuvrability becomes an advantage (Howland, 1974).

The most important marine predators of the Steller sea lion are killer whales and great white sharks (Riedman, 1990). Being significantly larger, these specialised swimmers can reach higher swimming speeds than sea lions. The only chance of survival for the sea lions consists of out-maneuvring their predators or escaping to a terrestrial refuge. Again, an unstable body design and good manoeuvring capabilities are a definite advantage in these situations (Howland, 1974).

From a kinematic perspective, the morphological features of the otariids present undeniable advantages and contribute to their superior manoeuvring capabilities compared to other marine mammals (Fish *et al.*, 2003). The rounded cross-section of the body of the sea lion facilitates rolling, one of the preparatory manoeuvres executed before performing a turn. The lack of lateral compression and dorsal fin, which would resist rolling, allows the sea lion to generate a rolling

moment with only a slight deflection of one of the pectoral flippers. Considering that rolling appears to be a necessary manoeuvre preceding a turn, it is advantageous — if not necessary — to reduce its duration and its cost in order to turn as quickly and as economically as possible. Having a flexible body allows the animal to bend in the direction of the turn and thus to reduce cross-flow and additional pressure drag during the manoeuvre. Bending the body while entering the manoeuvre with a non-zero speed also helps generating the rotational moment necessary to the turn (Tucker, 2000).

The large and very mobile pectoral flippers (average of 2180cm^2 , which represents 56% of the total flipper surface area — Table 2) of the Steller sea lion are positioned very close to the centre of gravity and play a crucial role during a turn. First, they act as independent deflectors and provoke the body roll; and second, they act as hydrofoils generating an important lift force towards the inside of the turn that changes the trajectory of the centre of gravity. They are also used to produce thrust during a bilateral stroke cycle that makes use of both lift and drag forces.

As shown by Feldkamp (1987a) for the California sea lion, the stroke cycle of the Steller sea lion is made up of a lift-based recovery phase and a power phase based on lift at first and ending up in a drag-based paddling movement. The recovery and power phases are performed during the turn. The recovery phase (or abduction) takes place during the first half of the turn and the power phase (or adduction) occurs during the second half of the turn. The greater the mobility of the pectoral flippers, the higher the amplitude of the stroke cycle — and therefore, the greater the thrust.

The pelvic flippers, with an average surface of 1700cm^2 (44% of the total flipper surface area — Table 2), serve two purposes. First, the interdigital web of the pelvic flippers is fully extended during the turn and resists an outward slip of the pelvic area. Second, as in many flying vertebrates, in which tails facilitate generating aerodynamic torques and substantially enhancing the quickness of body rotation (Dudley, 2002), they are used as a rudder to generate rotational moments.

Fish *et al.* (2003) measured morphological parameters on the flippers of two California sea lions, which present some interesting differences with the flippers of Steller sea lions. The total flipper area

of the California sea lion used in their study was a fraction of the average Steller sea lion flipper area (total flipper area: 0.227m² for the California and 0.389m² for the Steller sea lions), even though the animals in both studies were of comparable size (L=1.89m and mass=137.8kg for the male California and L=1.87m and mass=137.7kg on average for the Steller sea lions). This discrepancy in the projected area of the flippers might reflect an early development of the flippers in the Steller sea lion preceding the growth of their body, which is ultimately much larger and heavier than the California sea lion. Steller sea lions are the largest otariids with the males reaching up to 1,120kg and females to 350kg (Loughlin et al., 1987; National Marine Fisheries Service, 1992; Winship et al., 2001). In comparison, California sea lions grow up to a maximum of 390kg for males and 110kg for females (Riedman, 1990).

The difference in flipper area of the Steller and California sea lions also affects the kinetics of swimming. According to the lift equation ($L = \frac{1}{2} \rho A_p C_L U^2$), the lift force (L) is directly proportional to the surface area of the lift generating appendage (A_p) such that the larger the surface area, the higher the lift value (Hoerner and Borst, 1975). From a kinematic perspective, higher lift forces produced by the flippers translate into a more sudden change of trajectory and a quicker body rotation. Furthermore, the amount of water accelerated during the drag-based paddling movement of the pectoral flippers is related to the surface area of contact between the limb and the water. In this way, large flippers moved slowly produce thrust more efficiently than small flippers moved rapidly (English, 1976). Based only on flipper size, Steller sea lions would appear more manoeuvrable and more efficient swimmers than the California sea lions. However, this apparent advantage is probably negated by the fact that the larger Steller sea lions suffer from a substantially higher body drag.

Theoretically, the relatively small Steller sea lions that I studied should have been more manoeuvrable than the California sea lions that Fish et al. (2003) studied. However, my results do not support this hypothesis (see Fig. 13), perhaps because other parameters such as motivation levels played a role in the individual swimming performance of each animal. Another possible

explanation is that the aspect ratio of the pectoral flippers of the California sea lions was greater than that of the Steller sea lions, which could have resulted in the flippers of the California sea lions generating a greater lift force (Hoerner and Borst, 1975). Thus the degree of manoeuvrability between California and Steller sea lions may have been compensated by the difference in flipper shape between the two species.

In the case of large endotherms inhabiting the cold waters of the North Pacific Ocean and the Bering Sea, growing large swimming appendages will induce high thermo-energetic costs. In large adult animals that experience considerable inertial forces and require large control surface areas to maintain a certain degree of manoeuvrability, the biomechanical advantages drawn from these large flippers can be presumed to compensate for the thermoregulation costs. But the fact that younger and smaller animals — which experience less inertia — grow large flippers at an early age suggests that young animals also draw kinematic advantages from enlarged flippers, such as higher lift and thrust forces.

Kinematic analysis

Some aspects of the turning technique appear to be closely related, even though the different elements of the turning sequence show a certain degree of temporal variability. Table 3 illustrates that the first three movements of the sequence (notably the head displacement inside the turn, the abduction of the pectoral flippers and the start of the rolling movement of the body) do not follow a definite sequence and are interchangeable. Indeed, the position of the head is closely linked to the animal's field of view, whereby displacing the head inside the turn means committing to the manoeuvre. In other words, the animal moves its head inside of the turn and stops looking ahead, thereby creating a rotational moment (yaw) that initiates the rest of the manoeuvre. The turn is not irreversible at this point but demands adjustments to control yaw to reverse the movement, which is time consuming and induces a higher value of drag (see Tucker, 2000). Moreover, costs increase with increased speed, given that drag scales with the square of speed.

In a situation where the sea lion is uncertain about the recall signal, it would be advantageous to delay the head movement slightly before committing to the turn. It is worth mentioning that I never observed the rolling movement with my study animals before the start of the abduction of the pectoral flippers. This supports the hypothesis that rolling is controlled by an asymmetrical deflection of the pectoral flippers during the early stage of the abduction.

Directly following this initial phase (head movement, body roll, and start of the pectoral flipper abduction), the animal proceeds to arch its body dorsally, rotates its pelvic flippers outwards and extends the interdigital web of the pelvic flippers. These events often happen simultaneously, but when they do not, the body flexion precedes most of the time (Table 3).

The pelvic flippers serve two purposes during a manoeuvre: a) they control the movement of the posterior part of the body and prevent an outward slip and b) they generate rotational moment. When the animal's trajectory is rectilinear, the pelvic flippers are in a position that minimises exposed surface and therefore, friction drag. Rotating the pelvic flippers and exposing a maximum surface before the body starts manoeuvring is thus detrimental kinetically because of the undesired forces thus created. The onset of the pelvic flippers' movement is simultaneous to the start of the dorsal arch. At that point, the pelvic control surfaces start to be at an angle with the rest of the body and serve as a rudder. Furthermore, the body itself takes part in generating rotational moment when it arches into the turn (as suggested by Tucker, 2000). In short, the second phase of the turning sequence sees the growth of the centripetal force, which results in a change of swimming trajectory.

During Phase 3, the rolling movement and the abduction of the pectoral flippers stop at their maximum value. Both events are closely related and often happen simultaneously because the pectoral flippers create a large surface area that resists the rolling movement once they are stationary and maximally abducted. When both events are not simultaneous the flipper abduction always ends before the rolling movement (Table 3). This confirms the fact that the abduction of the pectoral flippers is responsible for the creation of the rolling movement.

Roll arises when the two control surface area generate different amounts of lift force (Hoerner and Borst, 1975). In the case of an aircraft, the ailerons are used to vary the amount of lift generated by each wing. In the absence of flipper ailerons, sea lions rely on other mechanisms to create this difference in lift force. One mechanism is to vary the angle of attack of each flipper, which affects lift force. The second mechanism acts not on the force directly, but on the distance between the flipper and the midline of the body. The greater this distance, the higher the moment of force. Therefore, rolling moment is created by abducting the outer flipper (i.e. the left flipper in a right turn) quicker than the inner flipper. This explains why rolling continues while the flippers are apparently fully abducted (i.e. the inner flipper that is away from the camera — Fig. 5 — was presumably still in motion). However, these hypotheses cannot be verified with the present recordings because the angle of view of the camera and the resolution of the images did not allow detailed analysis of the motion of the pectoral flippers.

During Phase 4, the body of the animal is maximally arched and the adduction (movement towards the midline of the body) of the pectoral flippers starts. While Phase 3 corresponded to a bout of minimum speed, this phase marks the beginning of the power stroke and the acceleration out of the manoeuvre. The adduction of the pectoral flipper is akin to the description of Feldkamp (1987a), and starts with a dorso-ventral power stroke (or power phase in Feldkamp's terminology). As noted by Feldkamp, such a movement creates a force oriented forwardly and dorsally. The timing of the onset of the pectoral adduction with, or slightly before, the maximum curvature of the body, allows the animal to make optimal use of the dorsal component of the force. At this point in the manoeuvre, the body is arched in a U-shape and the centre of mass is in the middle of the curved part of the trajectory. The timely onset of the dorsally oriented force therefore provides a useful centripetal component and a forward component. Performed earlier in the manoeuvre, the power stroke would leave the animal without control over the later stages of the turn (because the control surfaces would then be in a ventral position). Should the sea lion produce a late stroke, it would cause the animal to lose substantial amount of speed over the earlier stages of the turning manoeuvre during which no thrust is produced.

Phase 5 is the end of the manoeuvre. The body regains a straight orientation, and the adduction of the pectoral flippers reaches an end. The end of the body flexion often comes first as the animal slowly terminates the paddle phase. On these occasions, the end of the paddle phase consists of a passive adduction during which the flippers are brought up towards the ventral flanks of the animal. No thrust is produced during the paddle phase.

During Phase 6, the pelvic flippers exit the turn and regain a gliding position. The interdigital web remains extended as long as the pelvic flippers follow the curved trajectory. As soon as the angle between the midline of the body and the pelvic flippers returns to zero, they begin to rotate and the flipper surface area diminishes.

The turning sequence varied between the three animals I studied. First, all three displayed a strong directional preference. SL1 and SL3 always performed right turns whereas SL2 performed left turns. In the case of SL3, the side preference was potentially affected by her impaired eyesight on the left eye. She may have chosen the direction of the turn according to her field of view, which was mostly on her right side. For the other two animals, it is difficult to determine which one of the muscular, structural, or behavioural preferences mostly caused these directional preferences. Table 3 also shows that SL3 tended to start rolling only after her head and pectoral flippers were in motion, whereas SL1 and SL2 performed all three behaviours interchangeably. Here again, delaying the roll for SL3 may have been a behavioural adaptation to her impaired left eye. While the animals performed their manoeuvres they tended to keep visual contact with the trainers, and thus rolling the right side downwards in a right turn would have reduced SL3's field of view of the surface. For the same reason, all three animals rolled their heads less than the rest of their body during the turn. The degree of body roll, which was linked to the 3D swimming path during the turn, also varied between manoeuvres. If it was superior to 90 degrees, the animal tended to dive, and conversely if it was less than 90 degrees, the animal came closer to the surface.

On top of the variations of turning technique and sequence of actions, differences in the way certain movements were performed were observed. For instance, dorsal curvature varied with turning

radius, i.e. the larger the turning radius, the straighter the body (Fig. 7). In wide turns, which involved a low rotational moment, reducing the dorsal flexion and thus maintaining a streamlined body shape was advantageous because it limited the deceleration due to form drag. In tight turns however, the fast rotation of a non-flexing body would result in the creation of an important lateral pressure drag over the entire body length. In these situations, the curved body limited the lateral drag.

Abduction of the pectoral flippers was another variable that differed between animals. The general stroke technique can be divided in three major sections as presented by Feldkamp (1987a). During the recovery phase, the leading edge of the pectoral flipper is rotated outwards and brought forward and dorsally to varying degrees of sweep (i.e. angle between the midline of the flipper and the midline of the body) and dihedral (i.e. angle between the surface the flipper and the horizontal plane which contains the midline of the body). It follows the power phase during which the flippers are rotated inwards, and brought ventrally and backward. The stroke ends with the paddle phase during which the flippers continue to rotate inwards and move backwards and up, to rest on the ventral flanks of the animal. As mentioned above, the sweep and dihedral of the pectoral flippers vary in different turns. Particularly in very slow turns, the pectoral flippers are not fully abducted, i.e. the sweep does not approach 90 degrees (perpendicular to the midline of the body) and the dihedral is much less pronounced than during faster turns (Fig. 12).

According to the aerodynamic theory, lift and drag decrease with the distance between the lift-generating appendages and the body (Hoerner and Borst, 1975). For sea lions performing a slow turn, it is therefore advantageous to keep the pectoral flipper close from the body because a) it minimises the drag force and deceleration rate and b) the system does not require a high lift force to make its trajectory change. Finally, an important positive dihedral is synonymous to a stroke of high amplitude, which has been positively correlated with swimming speed (Feldkamp, 1987a) and therefore is unnecessary in a slow manoeuvre.

The turning technique of the California sea lions and Steller sea lions is strikingly similar (Fish et al., 2003) even though the California sea lion tends to perform the manoeuvre relatively faster (Fig. 13) and have slightly different morphological characteristics (see also English, 1976; Feldkamp, 1987a). Fish et al. (2003) noted that the attitude of the flippers in the California sea lion is highly variable and that the body of the animal is very flexible dorsally. It is this combination of highly mobile control surfaces and body flexibility that provides both species with an impressive array of manoeuvring capabilities without having to change the basic turning technique itself. For example, the inclination of the turning plane is determined by the rolling degree; the tightness of the turn varies with the body flexion; and the amplitude of the stroke influences speed. This is why the six phases of the general turning technique are quite consistent even though minor variations in the turning sequence are observed.

Sea lions are capable of fine-tuning parts of the turning sequence and adapting it to various situations, which gives the manoeuvring technique greater versatility (i.e. rolling without deviating from a rectilinear swimming path before starting the turning manoeuvre; controlling the rolling degree of the head to maintain visual contact with a particular object; modifying the rolling degree of the body to influence the animal's position in the water column at the end of the manoeuvre; varying the pectoral flipper stroke to control thrust production). Using this one general turning technique, the animal can therefore produce an almost infinite number of underwater manoeuvres. It is probably for this reason that the turning technique observed in other otariids, such as the California sea lion, is virtually identical to the one observed here.

In contrast, other marine mammals such as dolphins and whales do not have this manoeuvring capability and have to rely on a range of turning techniques whether they want to minimise turning radius, or deceleration, or maximise turning rate. The bottlenose dolphin for example relies on a "pinwheel" technique to minimise the turning radius of its mouth area and maximise its turning rate. Maresh et al. (2004) described the manoeuvre itself in these terms: "During the pinwheel, the animal appeared to keep its rostrum at a fixed point, and rapidly rotate its body around that point."

Such a manoeuvre essentially transforms all the translation speed of the system into rotational speed. But the dolphin thus offering its entire side to an important cross-flow probably pays a substantial price and endures a significant deceleration due to the creation of pressure drag around its body. Moreover, as thrust cannot be produced during the pinwheel itself, the animal has to "wait" until the end of the manoeuvre before it can re-accelerate. In the case of the sea lions, this delay is minimised as they rely on their large and mobile pectoral flippers to start accelerating half way through the turn.

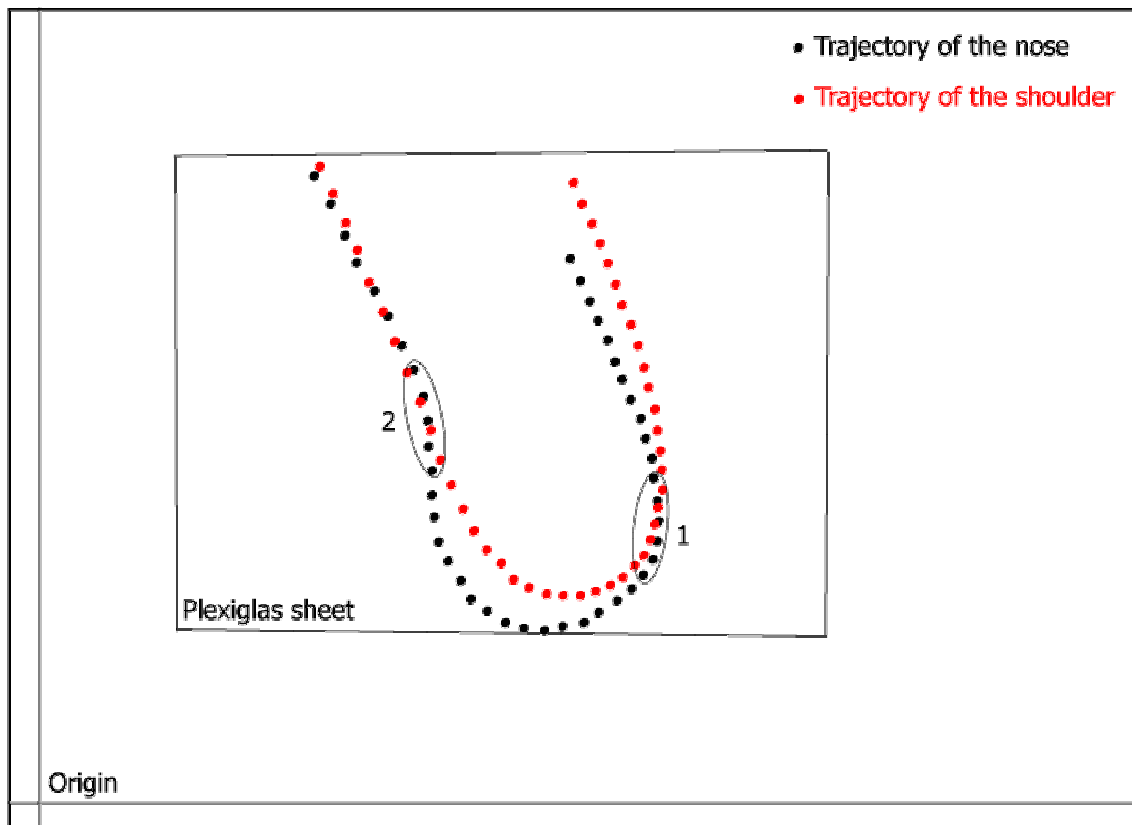


Fig. 10: Trajectory of the nose and shoulder of a sea lion performing a 180 degrees turn as filmed from above through a Plexiglas sheet. 1. The nose of the animal is displaced inside the turn and generates a trajectory that has an initial high curvature. 2. As the animal performs a stroke out of the manoeuvre and straightens its body, the dorsal component of the thrust force has to be corrected by a movement of the head and neck of the animal (represented here by the trajectory of the nose).

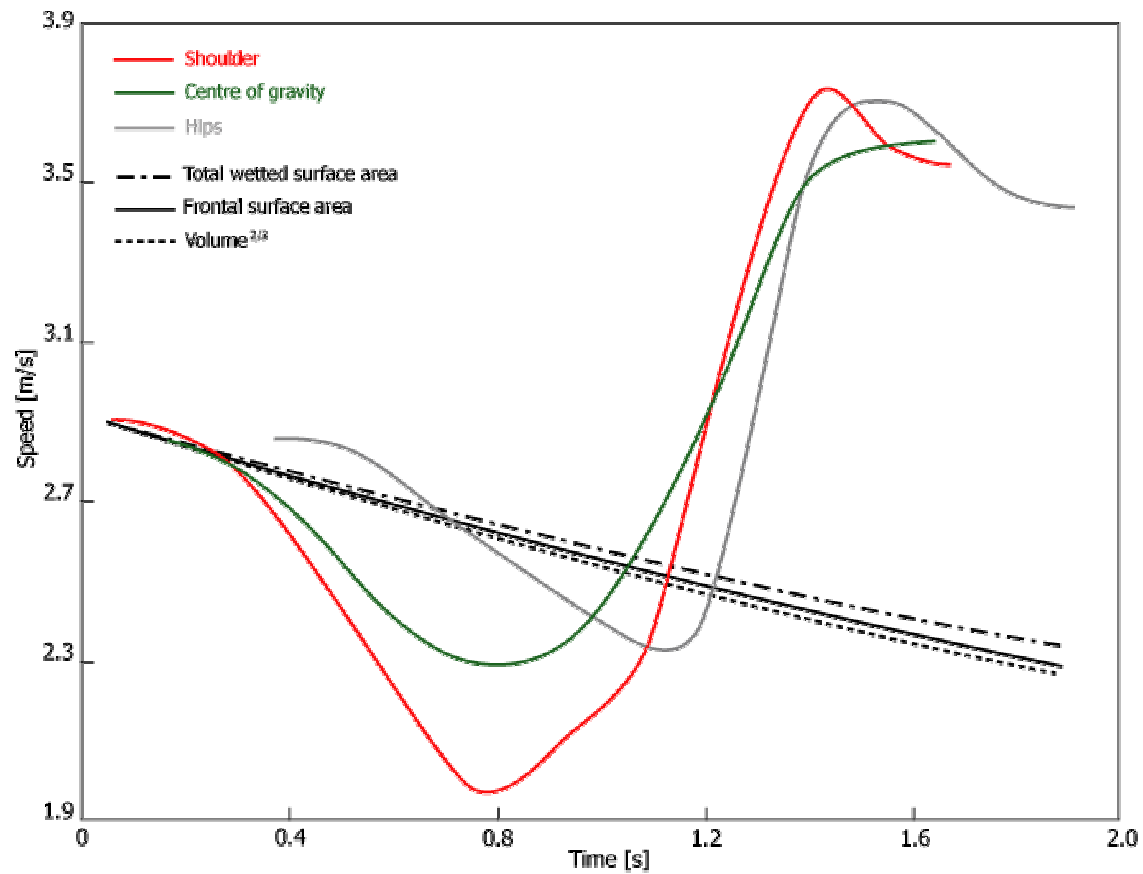


Fig. 11: Comparison of the speed profiles of the shoulder, centre of gravity, and hips markers of a Steller sea lion performing a 180 degrees turn with the predictions of a theoretical model of the speed variation of a Steller sea lion through an unpowered turn (Blake and Chan, in review). The black lines represent the model predictions. Each one of the three lines is based on a different referenced area, i.e. total wetted surface area, frontal surface area, or volume^{2/3}. For a discussion on the difference between reference areas, see Alexander (1990).

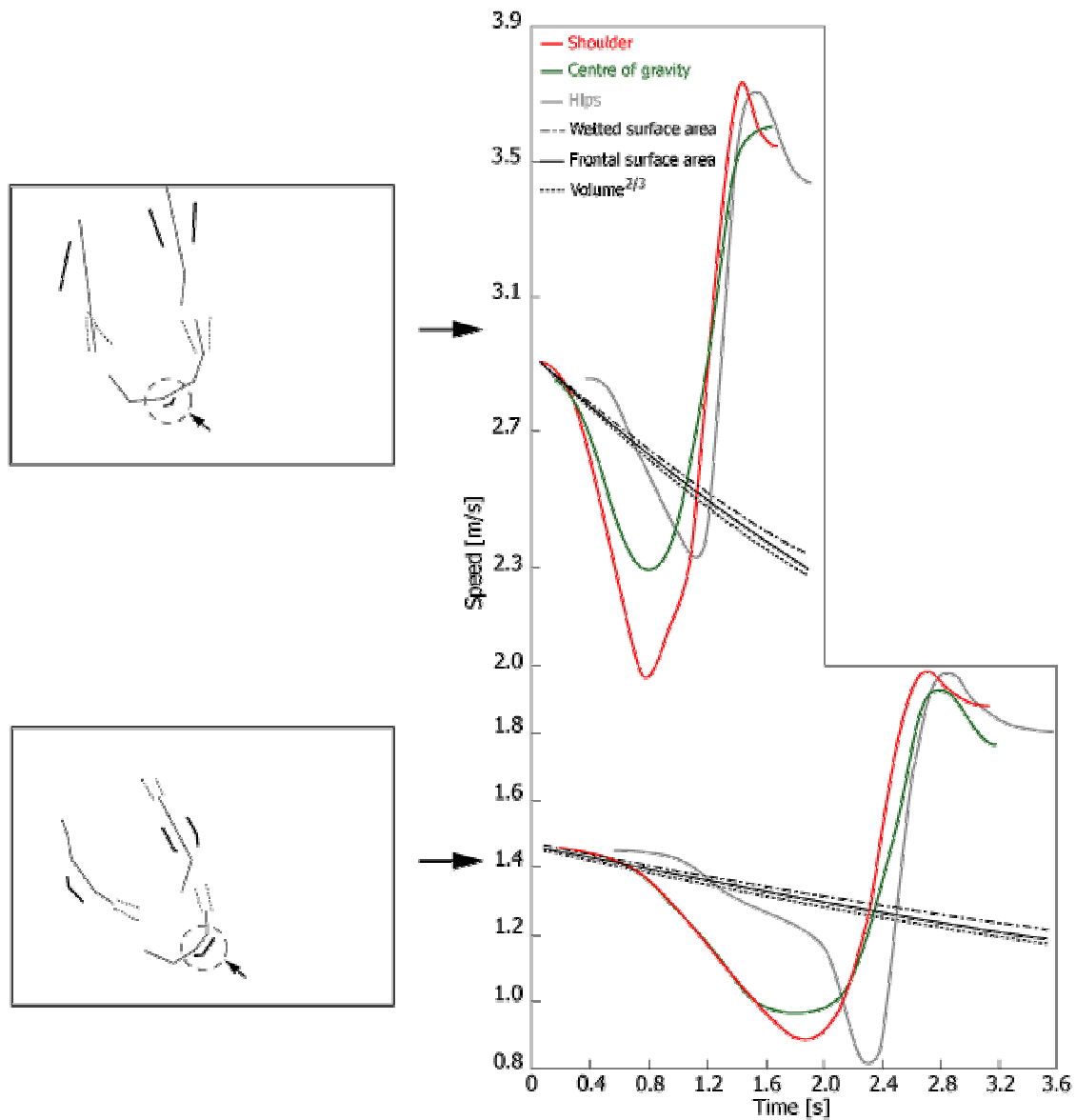


Fig. 12: Comparison of the speed profiles of the shoulder, centre of gravity, and hips markers of a Steller sea lion performing a fast and a slow 180 degrees turn. Note the difference in deceleration and acceleration as well as the average speed in both turns. The black lines on the graphs represent the predictions of the theoretical model of an unpowered turn (Blake and Chan, in review). The animal's midline and flipper position is indicated in the top-down view on the left-hand side. In turn A, the profile of the pectoral flipper in the middle of the turn is very short (indicated by the circle and the arrow), which means that the sweep angle of the pectoral flippers is close to 90 degrees. This is not the case in turn B, where the profile of the pectoral flipper is longer and does not move far from the body's midline (indicated by the circle and the arrow).

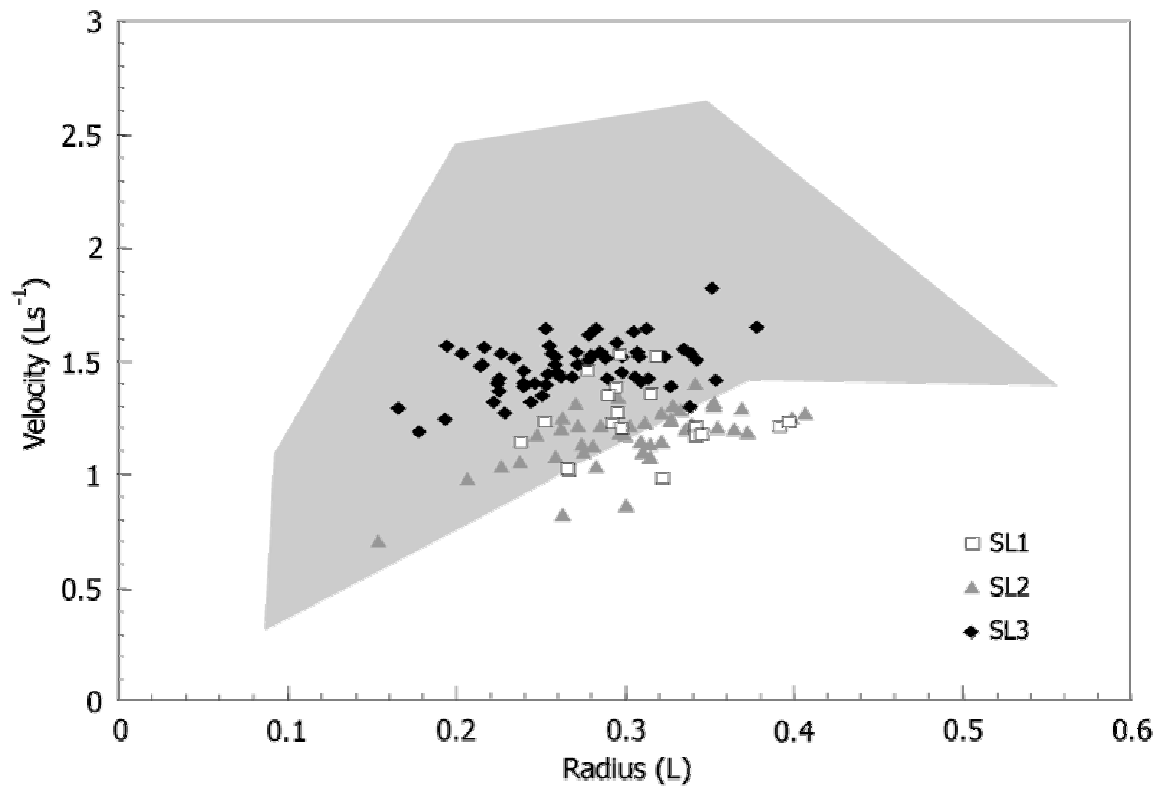


Fig. 13: Relative turning radius and average turning speed of three Steller sea lions in comparison to California sea lions (shaded area). Both turning radius and speed are expressed relative to the body length (L). The California sea lion data is taken from Fish et al. (2003).

Kinetic analysis

The speed profiles of most turns had a typical V-shape, preceded and followed by bouts of constant (or slightly decreasing) speed (Fig. 8), which corresponded to the glides at the beginning and at the end of the turns. As the animal started orienting its body inside of the turn and abducted its pectoral flippers, the deceleration became more pronounced (Fig. 8). This deceleration contrasts with the analysis of the foreflipper propulsion of the California sea lion (Feldkamp, 1987a), which showed that abduction of the pectoral flippers (i.e. the recovery phase) creates thrust.

The discrepancy between my findings and those of Feldkamp (1987a) might be because Steller sea lions and California sea lions use a different stroke technique. But the difference is more likely because Feldkamp studied sea lions swimming linearly against an incoming current. There are obvious advantages to producing thrust during as much of the stroke cycle as possible when swimming in a straight line. However, creating a forward force while preparing and adjusting for a manoeuvre can be destabilising.

Pectoral flippers serve a dual purpose of creating centripetal force and thrust during the turn. To perform a turn, the animal abducts and positions its control surfaces in a manner that will generate as much centripetal force as possible. This requirement is quite different from trying to generate as much forward thrust as possible (i.e. the flippers have a different angle of attack during the abduction, the degree of dihedral varies, etc.). Therefore, I suggest that otariids fine-tune the stroke technique to preferentially produce thrust during defined parts of the stroke cycle, i.e. by changing the angle of attack of the pectoral flippers, or the dihedral and amplitude of the stroke, or the sweep of the pectoral flippers, etc.

The adduction of the pectoral flippers of the Steller sea lion is composed of the two phases described by Feldkamp (1987a): the power phase followed by the paddle phase. In my study, I observed the latter when a passive glide followed the stroke but noted that it was omitted when the animal performed two successive strokes. In California sea lions swimming rectilinearly, most of the propulsive force comes from the paddle phase (Feldkamp, 1987a). In comparison, my results

showed that most of the thrust production occurs during the power phase. Acceleration stops at the end of the power phase, which indicates that the paddle phase produces little thrust. The fact that the animal by-passes the paddle phase altogether during a double stroke further supports this finding.

At the onset of the power phase, the animal is in the middle of the turn and its body is bent dorsally in a U-shape. At this point, the dorso-ventral movement of the pectoral flippers generates a dorsally oriented force, which points in the same direction as the anterior part of the body. This force is used to reaccelerate. In a linear situation, a dorsal force is wasteful hydrodynamically because of the heave (a dorso-ventral translation movement) thus created.

In order to correct the heave and maintain a rectilinear path, the animal has to spend energy correcting its trajectory by moving its head and neck (as noted at the end of a few turns I recorded — see Fig. 10). As previously mentioned, California sea lions asked to swim linearly against a current used the paddle phase to produce most of the thrust (Feldkamp, 1987a). During this phase, the main component of the thrust force is directed forward, which limits vertical movements. In the limited space of a swim mill, it makes most sense for the animal to use the paddle phase as much as possible. Again, this suggests that otariids modify their stroke cycle, i.e. emphasising the thrust production of one phase over the other, depending on their intended swimming trajectory.

Finally, in a manoeuvring situation, the power phase not only produces thrust, but also plays an important role in choosing the final swimming direction. For example, the sea lion can perform more than a 180 degree turn if it delays the onset of the power phase and maintains the dorsal arch longer. Conversely, if the animal maintains a low body curvature and performs a flipper stroke early on, it will turn less than 180 degrees.

Each body marker (shoulders, CG, hips) was seen to follow a slightly different trajectory, which was reflected in the different speed profiles (Figs 8, 12). The minimum speed of each body marker was reached before the middle of their respective curved trajectory. For the shoulders and the CG, the

minimum was reached before the start of the power phase. The hips on the other hand, reached their minimum speed later, approximately at the start of the power phase.

The minimum speed of the shoulders and the centre of gravity was often followed by a bout of constant or even slightly increasing speed (i.e. a 'flat' minimum), during which the pectoral flippers were abducted and motionless. This period sometimes carried through to the early stage of the power phase. This implies that the lift force generated off the still, abducted pectoral flippers can produce thrust before the start of the power phase. As the animal arches dorsally, the hips (representative of the posterior end of the body) move outside of the turn and their trajectory departs from the trajectory of the other two markers. This is a result of the rotational moment created by the displacement of the head inside the turn (for more on the effect of head displacement on rotation moment, see Tucker, 2000). As the body regains a straight position at the end of the turn, the trajectory of the hips crossed the two other tracks (Fig. 8), and the posterior end of the body therefore accelerated faster than the shoulders and CG.

The dorsal flexion and the extended pelvic flippers limit the outward motion of the posterior end of the body and reduce the overall deceleration. If the animal does not take these measures and remains in a straight position, the hips will rotate outwards, thus exposing the body to an important cross flow and pressure drag much like the bottlenose dolphins during a pinwheel manoeuvre (Maresh et al., 2004). In the case of a rigid object, the pressure drag created over the body's profile reduces both the translational and the rotational velocities because it acts on the entire length of the animal, on both sides of the centre of mass. As the turns become tighter and faster, the rotational and translational velocities increase as does the outward slip of the posterior end, thus inducing a high pressure drag, which scales with the square of speed.

In the case of the flexible Steller sea lion, the relationship between initial speed, turning radius, and posterior slip is not as straightforward as with a rigid body. In fact, such a clear relationship between these three variables would only be expected when the animal swims close to its maximum swimming capability, and cannot arch its back any further. I did not observe this in my study

because the test animals did not make use of their maximum dorsal flexion and did not swim at their maximum swimming capability (personal observation). Nevertheless, it is clear that the dorsal flexion allows animals to take advantage of the rotational moment generated over the anterior part of the body without suffering from the added pressure drag over the posterior end.

Stelle et al. (2000) determined that the average coefficient of hydrodynamic drag of 6 Steller sea lions passively gliding was 0.0046 (referenced to total wetted surface area), 0.044 (referenced to volume^{2/3}), or 0.080 (referenced to frontal surface area) at a mean Reynolds number of 5.52×10^6 . Recently, Blake and Chan (in review) developed a simple dynamic model, which predicts the speed of a submerged aquatic animal performing an unpowered turn as a function of time. By combining this model with the data of Stelle et al. (2000), I predicted a theoretical deceleration of 0.4 m/s^2 at an initial speed of 3 m/s (Fig. 11). However, my experimental data for the same initial speed indicates decelerations of 1.6 m/s^2 , 1.1 m/s^2 , and 0.8 m/s^2 for the shoulders, centre of gravity and hips respectively, all followed by an important acceleration (for average acceleration and deceleration values, see Table 4).

There are a number of potential explanations for the substantial divergence between observations and model predictions of deceleration rates. First, the observed sea lion turns were only unpowered during the first half of their manoeuvres. During the second half of the manoeuvres, the sea lions made use of the centripetal acceleration and performed a flipper stroke to create a positive acceleration that the model does not account for. Second, as Blake and Chan (in review) mention, the coefficient of drag (C_d) used in the model equations does not include the effect of drag on the control surfaces. Given the size and position of the control surfaces of the Steller sea lion during a turn, the amount of drag they induce is potentially important. Third, the C_d used in the model was obtained from instantaneous rates of deceleration during linear glides. In other words, it was assumed that C_d is the same during a manoeuvre and along a rectilinear swimming path. During a passive glide, a sea lion is motionless, keeping its pectoral flippers adducted along its ventral flanks, and reducing its pelvic flippers area. This configuration minimizes hydrodynamic drag (Stelle et al.,

2000) because it exposes a minimum amount of surface area to friction drag, and the sea lion maintains a streamlined shape. During a manoeuvre however, an animal generates a side force to deviate from its linear trajectory and this can only be accomplished by a body and/or a fin movement. It is therefore likely that C_d is greater during a manoeuvre due to these movements (Hughes and Kelly, 1996; Stelle et al., 2000; Webb, 1991). Unfortunately, most of the literature available on the coefficient of drag is related to passive drag (Bilo and Nachtigall, 1980; Feldkamp, 1987b; Williams and Kooyman, 1985).

The difference of drag experienced by a swimming sea lion in a passive glide and in a manoeuvre that involves both body and flipper movements is illustrated in the different deceleration rates of Figs 11 and 12. The body and flipper movements change the streamlining of the animal (its shape in relation to the incoming flow), thus influencing the value of C_d , and making the average deceleration rate at least 3 times greater than predicted by the model. The speed variation of a slow turn and a fast turn both diverge from the predictions of the theoretical model (Fig. 12) even though the movements of the flippers are not as pronounced during the slower manoeuvre. This suggests that body movements are mostly responsible for the deceleration at the beginning of the turn. Blake and Chan (in review) showed that their dynamic model predicts the deceleration of *Thunnus albacares* accurately. *T. albacares* is a specialized thunniform cruiser, which has limited body and fin movements, and cannot perform very tight turns ($0.47L$). In other words, their unpowered manoeuvres are closer to a linear glide than the manoeuvres of the flexible sea lions. This explains why the dynamic model yielded a better fit of the thunniforms than it did for Steller sea lions.

The normal acceleration (a_n) of the shoulders and the centre of gravity of the Steller sea lions started increasing during Phase 1 of the manoeuvring sequence (i.e. head displacement, roll, and flipper abduction). It continued to increase until reaching a maximum at the onset of the power phase of the pectoral flippers, and came back close to zero during Phase 5 of the sequence, at the end of the power phase. The maximum value of normal acceleration never exceeded 20m/s^2

(approximately 2g), a value much lower than previously evaluated for otariids (notably 5.13g for the California sea lion - Fish et al., 2003).

The difference between these maximum acceleration values in different species of otariids might be explained in two ways. First, my experimental design may not have forced the Steller sea lions to reach their highest performance level — and even the upper 20% of my data may not be representative of the extreme manoeuvring and swimming capabilities of the animals (personal observations). Up to some extreme values, swimming speed and turning radius are under behavioural control and thus are principally influenced by motivation levels. This may explain why Fish et al. (2003) obtained higher relative velocities and turning radii for California sea lions (Fig. 13) even though their experimental setup was similar to ours.

A second possible explanation is that Fish *et al.* (2003) used the equation $a_c = a_n = \frac{U^2}{r}$ and the average turning speed to calculate centripetal acceleration (equal to the normal acceleration, assuming the turn follows a circular trajectory). Given that the maximum values of a_n are reached during the time of minimum speed, the equation will tend to overestimate the maximum centripetal acceleration for average values of speed. Based on the difference between the average speed and the minimum speed of the 195 turns I observed, I assess that the overestimation of maximum a_c was about 30%.

The maximum tangential acceleration (a_t) closely followed the maximum of a_n , thereby illustrating the dual role of the power phase — to reposition the body at the end of the turn and accelerate. The hips also followed the same progression after a short delay (as seen by the peak in a_n following the peak in a_t). In all of the turns that I recorded, the maximum normal acceleration was systematically greater than the maximum tangential acceleration. In other words, it took a greater force to maintain a curved trajectory and resist slip than to reaccelerate. In the absence of dorsal keels or structures that help to create this important centripetal force, sea lions (as well as penguins - Hui,

1985) depend on their large pectoral flippers, which explains why they have to roll to appropriately position these control surfaces.

CONCLUSIONS

Steller sea lions use the same technique to turn as has been reported for another otariid, the California sea lion (Fish et al., 2003). However, significant new information was obtained about the techniques employed by otariids by jointly analysing both kinematic and kinetic parameters of the turns performed by Steller sea lions.

First, the data show that otariids are one of the most manoeuvrable marine mammals even though they deploy a consistent turning technique. Changes in initial speed or turning angle do not affect the turning sequence. Rather, Steller sea lions vary the duration and intensity of movements within the turning sequence, and thus have an almost infinite number of options to determine directionality.

Second, the majority of observed sea lion turns had a V-shape speed pattern, which reflects the partially powered manoeuvring style of otariids. Dorsal flexion and abduction movements of the large pectoral flippers inflict more drag compared to a linear glide during the first stages of a manoeuvre. This translates into increased deceleration, which becomes less pronounced once the pectoral flippers are fully abducted. The maximum centripetal acceleration is reached slightly after the minimum speed at the beginning of the power phase of the pectoral flipper stroke. Finally, the power phase of the pectoral flipper stroke causes the animal to accelerate at the end of the turn.

A third notable finding was that my assessment of flipper movement of otariids during a turn (pectoral propulsion) differed significantly from the results obtained by Feldkamp (1987a) for linearly swimming animals. I found that the abduction of the pectoral flippers (also known as the recovery phase) by animals preparing for a turn did not produce thrust as indicated by the considerable

deceleration I observed. However, Feldkamp (1987a) found that thrust was generated during the recovery phase.

During the second part of the turn, I found that most of the thrust was produced during the power phase of the flipper stroke. Little thrust was created during the paddle phase, to the point that it would be skipped altogether during a double stroke. In contrast, Feldkamp (1987a) found that the paddle phase produced most of the thrust generated over the entire stroke cycle in linearly swimming animals. This could suggest that Steller sea lions and California sea lions have a different stroke technique. However, given the orientation of the forces during the stroke cycle and the great mobility of the thrust-producing appendages, it is more likely that both species modify their stroke technique according to the situation (i.e. linear versus curved swimming trajectory).

A final noteworthy finding stemming from my data is that Steller sea lions are not as manoeuvrable as California sea lions in terms of pure turning performance (Fish et al., 2003). However this conclusion may need further scrutiny given that the turning performance of the sea lions in both experimental setups may have depended heavily on the motivation level of the study animals.

REFERENCES

- Alexander, D. E.** (1990). Drag coefficients of swimming animals: effects of using different reference areas. *Biological Bulletin* **179**, 186-190.
- Bilo, D. and Nachtigall, W.** (1980). A simple method to determine drag coefficients in aquatic animals. *Journal of Experimental Biology* **87**, 357-359.
- Blake, R. W.** (1977). On ostraciiform locomotion. *Journal of the Marine Biological Association of the United Kingdom* **57**, 1047-1055.
- Blake, R. W.** (2004). Fish functional design and swimming performance. *Journal of Fish Biology* **65**, 1193-1222.
- Blake, R. W. and Chan, K. H. S.** (in review). A simple model of the dynamics of turning in aquatic animals. *Journal of Fish Biology*.
- Blake, R. W., Chatters, L. M. and Domenici, P.** (1995). Turning radius of yellowfin tuna (*Thunnus albacares*) in unsteady swimming manoeuvres. *Journal of Fish Biology* **46**, 536-538.
- Domenici, P.** (2003). Habitat, body design and the swimming performance of fish. In *Experimental Biology Reviews. Vertebrate biomechanics and evolution*, eds V. L. Bels A. Casinos and J.-P. Gasc), pp. 137-160. Oxford: BIOS Scientific Publishers Ltd.
- Domenici, P. and Blake, R. W.** (1997). The kinematics and performance of fish fast-start swimming. *Journal of Experimental Biology* **200**, 1165-1178.
- Domenici, P. and Blake, R. W.** (2000). Biomechanics in behaviour. In *Biomechanics in Animal Behaviour*, eds P. Domenici and R. W. Blake), pp. 1-17. Oxford: BIOS Scientific Publishers Ltd.
- Domning, D. P. and De Buffrénil, V.** (1991). Hydrostasis in the sirenia: quantitative data and functional interpretations. *Marine mammal science* **7**, 331-368.
- Dudley, R.** (2002). Mechanisms and implications of animal flight maneuverability. *Integrative and Comparative Biology* **42**, 135-140.
- English, A. W.** (1976). Limb movements and locomotor function in the California sea lion (*Zalophus californianus*). *Journal of Zoology, London* **178**, 341-364.
- Feldkamp, S. D.** (1987a). Foreflipper propulsion in the California sea lion, *Zalophus californianus*. *Journal of Zoology, London* **212**, 43-57.
- Feldkamp, S. D.** (1987b). Swimming in the California sea lion: morphometrics, drag and energetics. *Journal of Experimental Biology* **131**, 117-135.
- Firth, H. R. and Blake, R. W.** (1991). Mechanics of the startle response in northern pike, *Esox lucius*. *Canadian Journal of Zoology* **69**, 2831-2839.
- Fish, F. E.** (1993). Influence of hydrodynamic design and propulsive mode on mammalian swimming energetics. *Australian Journal of Zoology* **42**, 79-101.

- Fish, F. E.** (1997). Biological designs for enhanced maneuverability: analysis of marine mammal performance. In *Tenth International Symposium on Unmanned Untethered Submersible Technology: Special Session on Bio-engineering Research Related to Autonomous Underwater Vehicles*, (ed. A. a. ONR). Durham.
- Fish, F. E.** (2002). Balancing requirements for stability and maneuverability in cetaceans. *Integrative and Comparative Biology* **42**, 85-93.
- Fish, F. E., Hurley, J. and Costa, D. P.** (2003). Maneuverability by the sea lion *Zalophus californianus*: turning performance of an unstable body design. *Journal of Experimental Biology* **206**, 667-674.
- Fish, F. E., Innes, S. and Ronald, K.** (1988). Kinematics and estimated thrust production of swimming harp and ringed seals. *Journal of Experimental Biology* **137**, 157-173.
- Gerstner, C. L.** (1999). Maneuverability of four species of coral-reef fish that differ in body and pectoral-fin morphology. *Canadian Journal of Zoology* **77**, 1102-1110.
- Harper, D. G. and Blake, R. W.** (1990). Prey capture and the fast-start performance of the rainbow trout *Salmo gairdneri* and the northern pike *Esox lucius*. *Journal of Experimental Biology* **150**, 321-342.
- Hoerner, S. F. and Borst, H. V.** (1975). Fluid dynamic lift. Brick Town, N.J.: Mrs. Liselotte A. Hoerner.
- Howland, H. C.** (1974). Optimal strategies for predator avoidance: the relative importance of speed and maneuverability. *Journal of Theoretical Biology* **47**, 333-350.
- Hughes, N. F. and Kelly, L. H.** (1996). A hydrodynamic model for estimating the energetic cost of swimming maneuvers from a description of their geometry and dynamics. *Canadian Journal of Fisheries and Aquatic Sciences* **53**, 2484-2493.
- Hui, C. A.** (1985). Maneuverability of the Humboldt penguin (*Spheniscus humboldti*) during swimming. *Canadian Journal of Zoology* **63**, 2165-2167.
- Loughlin, T. R., Perez, M. A. and Merrick, R. L.** (1987). *Eumetopias jubatus*. In *Mammalian Species Account no.283*, pp. 1-7: The American Society of Mammalogists.
- Maresh, J. L., Fish, F. E., Nowacek, D. P., Nowacek, S. M. and Wells, R. S.** (2004). High performance turning capabilities during foraging by bottlenose dolphins (*Tursiops truncatus*). *Marine mammal science* **20**, 498-509.
- Merrick, R. L., Chumbley, M. K. and Byrd, G. V.** (1997). Diet diversity of Steller sea lions (*Eumetopias jubatus*) and their population decline in Alaska: a potential relationship. *Canadian Journal of Fisheries and Aquatic Sciences* **54**, 1342-1348.
- National Marine Fisheries Service.** (1992). Recovery Plan for the Steller Sea Lion (*Eumetopias jubatus*). (ed. Steller Sea Lion Recovery Team for the National Marine Fisheries Service), pp. 92. Silver Spring, Maryland.
- Norberg, U. and Rayner, J. M. V.** (1987). Ecological morphology and flight in bats (Mammalia: Chiroptera): Wing adaptations, flight performance, foraging strategy and echolocation. *Philosophical Transactions of the Royal Society B* **316**, 335-427.

- Nowacek, D. P.** (2002). Sequential foraging behaviour of bottlenose dolphins, *Tursiops truncatus*, in Sarasota Bay, Fl. *Behaviour* **139**, 1125-1145.
- Ponganis, P. J., Ponganis, E. P., Ponganis, K. V., Kooyman, G. L., Gentry, R. L. and Trillmich, F.** (1990). Swimming velocities in otariids. *Canadian Journal of Zoology* **68**, 2105-2112.
- Riedman, M.** (1990). *The Pinnipeds: Seals, Sea Lions, and Walruses*. Berkeley, CA: University of California Press.
- Rosen, D. A. S. and Trites, A. W.** (2004). Satiation and compensation for short-term changes in food quality and availability in young Steller sea lions (*Eumetopias jubatus*). *Canadian Journal of Zoology* **82**, 1061-1069.
- Schrank, A. J., Webb, P. W. and Mayberry, S.** (1999). How do body and paired-fin positions affect the ability of three teleost fishes to maneuver around bends? *Canadian Journal of Zoology* **77**, 203-210.
- Sinclair, E. H. and Zeppelin, T. K.** (2002). Seasonal and spatial differences in diet in the western stock of Steller sea lions (*Eumetopias jubatus*). *Journal of Mammalogy* **83**, 973-990.
- Stelle, L. L.** (1997). Drag and energetics of swimming in Steller sea lions (*Eumetopias jubatus*). In *Department of Zoology*, pp. 84. Vancouver: University of British Columbia.
- Stelle, L. L., Blake, R. W. and Trites, A. W.** (2000). Hydrodynamic drag in Steller sea lions (*Eumetopias jubatus*). *The Journal of Experimental Biology* **203**, 1915-1923.
- Tucker, V. A.** (2000). Gliding flight: drag and torque of a hawk and a falcon with straight and turned heads, and a lower value for the parasite drag coefficient. *Journal of Experimental Biology* **203**, 3733-3744.
- Walker, J. A.** (2000). Does a rigid body limit maneuverability? *Journal of Experimental Biology* **203**, 3391-3396.
- Wardle, C. S.** (1975). Limit of fish swimming speed. *Nature* **255**, 725-727.
- Webb, P. W.** (1977). Effects of median-fin amputation on fast-start performance of rainbow trout (*Salmo gairdneri*). *Journal of Experimental Biology* **68**, 123-135.
- Webb, P. W.** (1978). Fast-start performance and body form in seven species of teleost fish. *Journal of Experimental Biology* **74**, 211-226.
- Webb, P. W.** (1983). Speed acceleration and maneuverability of 2 teleost fishes. *Journal of Experimental Biology* **102**, 115-122.
- Webb, P. W.** (1984). Body form, locomotion and foraging in aquatic vertebrates. *American Zoologist* **24**, 107-120.
- Webb, P. W.** (1991). Composition and mechanics of routine swimming of rainbow trout, *Oncorhynchus mykiss*. *Canadian Journal of Fisheries and Aquatic Sciences* **48**, 583-590.
- Weihls, D.** (1973). The mechanism of rapid starting of slender fish. *Biorheology* **10**, 343-350.

- Weihs, D.** (2002). Stability versus maneuverability in aquatic locomotion. *Integrative and Comparative Biology* **42**, 127-134.
- Williams, T. M. and Kooyman, G. L.** (1985). Swimming performance and hydrodynamic characteristics of harbor seals *Phoca vitulina*. *Physiological Zoology* **58**, 576-589.
- Winship, A. J., Trites, A. W. and Calkins, D. G.** (2001). Growth in body size of the Steller sea lion. *Journal of Mammalogy* **82**, 500-519.